DLR-IB-AT-KP-2016-198

Further developments in Filtered Rayleigh scattering for the determination of the turbine inlet temperature distribution in gas power stations

Masterarbeit

Manuel Bridger

Deutsches Zentrum
DLR für Luft- und Raumfahrt

Further developments in Filtered Rayleigh scattering for the determination of the turbine inlet temperature distribution in gas power stations

Master thesis by
Manuel Bridger

Supervised by:

University Bielefeld - Faculty of Physics:
Prof. Dr. Thomas Huser

University Regensburg - Faculty of Physics:
Prof. Dr. John Lupton

DLR Cologne - Institute of Propulsion Technology:
Dr. rer. nat. Guido Stockhausen
Dipl.-Ing. Ulrich Doll

30. January 2016

Gefördert durch:

Bundesministerium für Wirtschaft und Technologie

aufgrund eines Beschlusses des Deutschen Bundestages

Universität Regensburg

Universität Bielefeld

DLR

Contents

List of Figures

1 Introduction

It is very difficult to precisely measure thermodynamic parameters like temperature, pressure and flow velocity in extreme environments as they exist in a running gas power turbine. There is conventional equipment with which these parameters may be measured one after another, but they all have various disadvantages. There are probe based methods which use different probes to measure one thermodynamic parameter at a time. These probes need to be inserted into the gas flow in which challenging conditions prevail, like temperatures up to 1800 K, pressures up to 30 bar and corrosive gases. Therefore they are subject to great stress and also slightly disturb the gas flow.
To not affect the gas flow by probes and be able to quantify thermodynamic parameters, optical measurement methods can be used. Newly developed methods in this matter guide a laser beam through a fiber into the connecting link between the combustion chamber and the vanes of the turbine. However due to the hot gas flowing through this channel, these vanes are thermally extremely charged, hence reaching temperatures of up to 1400 K as can be seen in figure 1. This immense temperature load brings the vanes to glow extensively bright due to black body radiation. Therefore the use of optical measurement methods is in principle almost impossible since this radiation outshines the optically induced signal. To be able to perform optical measurements at all, the detector system for this signal needs to suppress the black body radiation of the hot vanes far enough to distinguish between these background signals and the measurement signal. Furthermore the most interesting section of the gas flow is right before it encounters the vanes of the turbine in order to determine the turbine inlet temperature distribution. Due to that the inducing laser beam for optical measurements needs to be placed directly in front of the vanes, making the detection of the signal even more difficult.

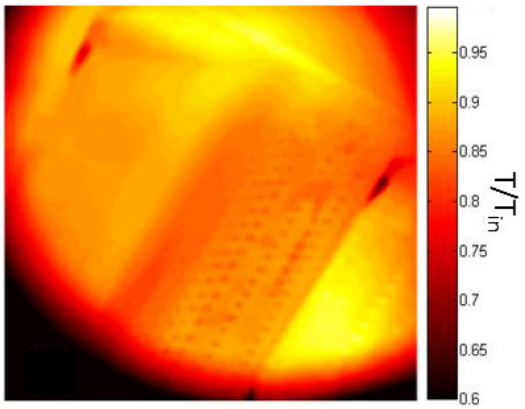

Figure 1: Infrared picture of a vane surface under stress [Bon12]

An optical measurement method to determine the flow velocity is called "Particle Image Velocimetry" (PIV). This technique introduces new seeding particles into the gas flow which are illuminated with multiple short laser pulses and then photographed with cameras. With this series of images, the

movement of the particles can be reconstructed. However, to successfully use PIV, clear images of the seeding particles need to be taken to accomplish reliable results. Hence this method comes with difficulties since optical measurements in gas power stations must be performed endoscopically.
An optical method to determine the temperature, measures the "Laser Induced Fluorescence" of OH^- ions (OH-LIF). OH-LIF uses UV light to excite re.pngsonant transitions of the molecules which hence radiate luminescence light. This response is used to determine the inner energy distribution of the molecules, which directly corresponds to the temperature in the area of interest. However UV light fibers can transport light only up to a few Watts of power without breaking and are therefore limiting the amount of maximal intensity.
A promising optical method is the "Filtered Rayleigh Scattering" (FRS) technique. The concept of this approach is to guide a laser beam through a fiber into the link between the combustion chamber and the vanes of the gas power turbine to measure the spectral response of the molecules. The largest share of the response is caused by Rayleigh-, Mie- and geometrical scattering (Reflex light). To be able to clearly measure the Rayleigh signal which has the same wavelength as the other two factors, their contribution can be sorted out with a molecular filter. Using this method, temperature, pressure and flow velocity can be determined simultaneously along the laser beam. It is even possible to use this method to scan a plane within the chamber, if the laser is expanded to a laser sheet. However there is a problem with this measurement method as well. The glowing hot vanes of the turbine produce a black body signal which outshines the Rayleigh light from the laser by far, making FRS measurements impossible.
In this thesis two different approaches will be tested to reduce this interfering signal sufficiently that FRS measurements can be performed even with a 1400 K thermal background. The first approach is to use a 1 nm thin bandpass filter to absorb a large part of this contribution in combination with a pulsed 250 mJ/pulse laser system. Due to the pulsed operation of the system it is possible to use high laser powers in short time ranges and therefore improving the relation between Rayleigh light and background light by exposing the detector only as long as a laser pulse is present.
The second approach is to use a 5 W continuous wave laser system together with an even thinner 0.15 nm bandpass filter. This improvement may be sufficient to lower the background signal enough for FRS measurements to take place.

2 Theoretical Background

2.1 Rayleigh-scattering

In principle scattering processes between electromagnetic waves and spherical particles of arbitrary size are described by the Lorenz-Mie-theory. To be in accordance with this theory, the electromagnetic wave has to fulfill the wave equation during the scattering process as well as afterwards. In addition to that, the tangential component of the field within the scattering object has to merge continuously into the field outside this area [Vor02]. This complex problem is only rarely solvable analytically, so that it is often necessary to use calculation programs for an approximated solution. However, the potency of the theory becomes clear as one looks at a limiting case of the problem, for example if the size of the particles are small in comparison to the wavelength of the incoming light. In this case the scattering process is called Rayleigh-scattering in remembrance of John William Strutt (1842-1919), who was ennobled in the year 1873 to Lord Rayleigh.
For those small particles the differential scattering cross section can be written as [Mil01]:

$$\frac{\partial\sigma}{\partial\Omega} = \frac{9\pi^2 V^2}{\lambda^4}\left(\frac{n^2-1}{n^2+2}\right)^2 \sin^2\theta \tag{1}$$

In this equation θ denotes the angle between the induced dipole moment $\vec{p} = \alpha\vec{E}_i$ and the scattered wave of the electrical field vector $\vec{E}_s$. V is the volume and n is the refractive index of the particle. Also visible in the equation is that the differential scattering cross section is dependent of λ^{-4}. It is due to this fact that the sky is blue, since blue light is scattered approximately 10 times more in the atmosphere than red light. So that the direct beam from the sun is visible yellow and the scattered blue light dyes the sky blue. The scattering is a result of the interaction of the electric field E_i of the light wave and the electrons of the particle at the submicroscopic level. The latter are excited by the E-field and begin to oscillate, therefore emitting the energy like a Hertzian dipole. Since there is no loss of energy during the process, the scattering is elastic. In figure 2 the intensity of the scattering dependent of the direction is visualized. If the laser beam is polarized in the z-direction, then no Rayleigh scattering light will be visible along this axis.

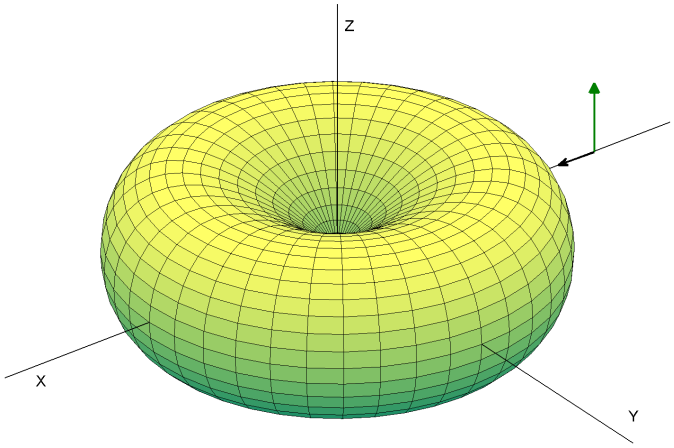

Figure 2: Polar diagram of the intensity field around the dipole aligned with the z-axis. At any point of the surface, the radial distance from the origin squared is proportional to the magnitude of the field measured at that location. [Mil01]

2.2 Tenti model

Rayleigh scattering from gas molecules ensembles is influenced by the thermodynamic parameters, pressure, density, temperature and flow velocity. If the temperature is raised, the thermal movement of the molecules increases. As they have higher speeds in random directions, the spectrum of Rayleigh light broadens due to the Doppler effect. Since there will be particles with higher speeds towards and away from the exciting light, the effective wavelength will be longer or shorter respectively. Therefore, at pressures around 1 bar, the spectral distribution around the excitation wavelength will turn into a Gaussian distribution with raising temperatures as can be seen in figure 3. If an examined ensemble of molecules moves in a specific direction, it has an average velocity which causes the Rayleigh spectrum to be shifted in frequency relative to this velocity. The signal strength is proportional to the density, as the number of scattering centers increases. Therefore the laser light is more often scattered and the intesity oft the Rayleigh light rises. The pressure influences the Rayleigh spectrum by changing the form. This effect will be discussed later in this chapter.
The shape of the Rayleigh spectrum due to these influences is best described by the Tenti S6 model [Tenti74], which is intended to predict the scattering spectrum of a two atomic molecule. Since air consists almost completely of two atomic molecules like N_2 and O_2, it is the best choice for experiments under normal conditions. This model introduces two dimensionless parameters [Tenti74]:

$$x = \frac{\omega}{\sqrt{2}Kv_0} \tag{2}$$

$$y = \frac{nk_BT}{\sqrt{2}Kv_0\eta} = \frac{p}{\sqrt{2}Kv_0\eta} \tag{3}$$

ω denotes the angular frequency shift between scattered and incident light, n is the particle density, p and T are the gas pressure and temperature. η is the shear viscosity. $K = |\vec{K}_s - \vec{K}_0| = \frac{4\pi}{\lambda}\sin(\phi/2)$ is the magnitude of the interacting wave vector (with $\vec{K}_s$ and $\vec{K}_0$ being the wave vectors of the incident and scattered light), λ is the wavelength of the incident light, ϕ is the scattering angle and $v_0 = \sqrt{k_BT/m}$ is the thermal velocity (with k_B being the Boltzmann constant and m the molecular mass). This concludes that x is the optical frequency shift and y the collision frequency [Wit11]

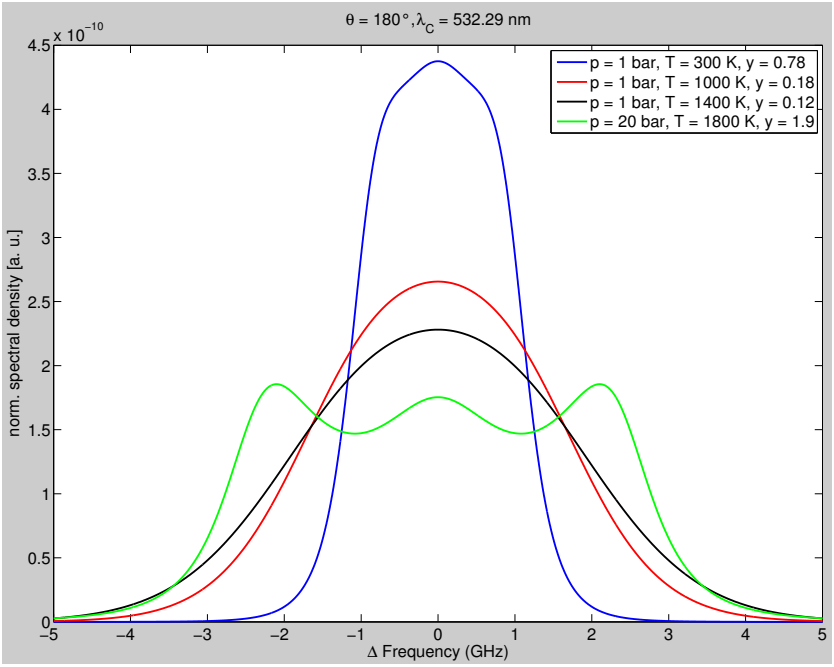

Figure 3: Theoretical Rayleigh profiles for different y-parameters in air. The y-axis is normed in such a way that the full space integral of the function gives 1.

Since the y-Parameter is very important for the shape of the Rayleigh profile, three different scattering regimes have been defined:

1. Knudsen regime: $y \ll 1$
2. Kinetic regime: $y \approx 1$
3. Hydrodynamic regime: $y \gg 1$

The Knudsen regime describes the form of the spectrum if the temperature is very high and/or the pressure is very low. In this regime the mean free path between collisions is much higher than the acoustic wavelength, therefore the thermal motion of the molecules dominates the spectrum and the form merges with the Gaussian spectrum.
In the opposite case, the Hydrodynamic regime, low temperature and/or high pressure, the mean free path between collisions is very short, so that acoustic effects contribute to the form of the spectrum very much. Because of that two Brillouin side peaks emerge at lower (Stokes component) and higher (anti-Stokes component) frequencies. This frequency shift is the result of a Doppler effect based on the acoustic wave vector $|\vec{K_a}| = |\vec{K}| = 2|\vec{K_0}|\sin(\theta/2)$. This

implies that the shift of the Brillouin side-peaks in the frequency domain f_b can be written as [Gu13]:

$$f_b = 2nf\frac{a}{c}\sin\left(\frac{\theta}{2}\right) \tag{4}$$

with n being the index of refraction, c the velocity of light in vacuum, a the velocity of sound and f the frequency of the incident light, depending on the scattering geometry.
The kinetic regime is the one that describes all applications at atmospheric conditions. For example at "normal" room conditions (T = 298 K ≈ 25 °C, p = 1 bar) with a wavelength of $\lambda = 532.29$ nm, the resulting y-parameter is 0.78. The Tenti model was designed especially for this case on the basis of approximate solutions of the linearized Boltzmann equation [Tenti74].

2.3 Filtered Rayleigh-scattering (FRS)

The measurement technique Filtered Rayleigh Scattering under harsh conditions is the main topic of this thesis. This measurement method can be explained by following steps:

1. The laser illuminates the molecules which then emit light due to Rayleigh scattering
2. This Rayleigh scattered light is "filtered" by a molecular filter
3. The luminescence of this molecular filter as well as inelastic background light is blocked by an interference filter
4. The residual light is measured by a camera
5. From this signal value pressure, temperature and flow velocity can be derived

2.3.1 Motivation for FRS

As mentioned before in chapter 2.2, the Rayleigh scattered light is influenced and therefore holds information about different properties of the ensemble, namely pressure, temperature, density and velocity. Usually it is difficult to measure only the Rayleigh signal for itself, since other light phenomena like Mie- and geometrical-scattered light are magnitudes stronger than the Rayleigh signal. However these influences have the same spectral bandwidth as the laser light. In contrast to that, the Rayleigh scattered light is spectrally

broadened because of the mechanisms mentioned in chapter 2.2. This fact is used by the molecular filter. It serves as an extremely fine notch filter for the scattered light. Therefore the laser frequency has to be set close enough to a strong absorption line of the molecular filter. That way a large part of the Rayleigh signal is lost, but the Mie- and geometrical-scattered light can be suppressed greatly, as can be seen in the figures 4 and 5.

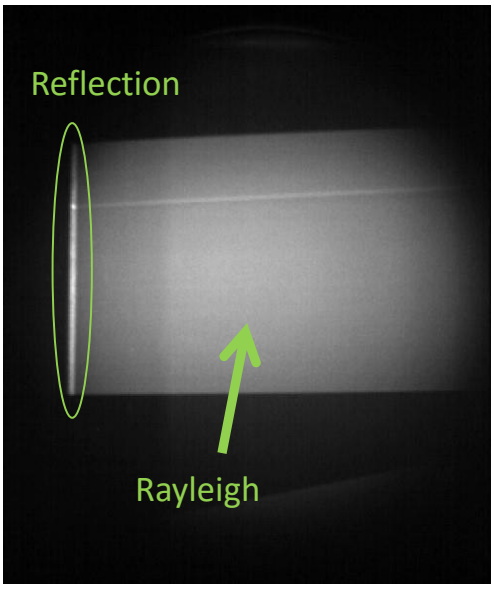

Figure 4: A laser sheet with the wave number of 18788.336 cm^{-1} is pointed at a blackened metal surface (left). But since the molecular filter has a strong absorption line at that laser frequency, the complete contribution caused by Mie-scattering and the greatest part of the primary reflection is suppressed so that the Rayleigh light can still be measured (center).

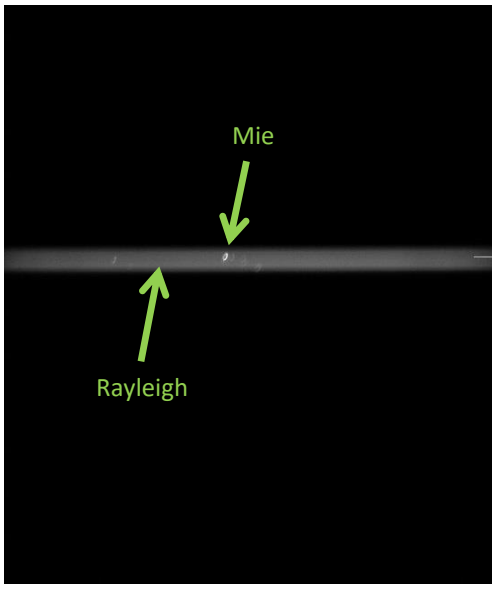

Figure 5: An unobstructed laser beam with the wave number of 18786.75 cm^{-1} is at the flank of another strong absorption line of the molecular filter. At this point the Mie-signal is not suppressed strongly enough by the filter and therefore signal peaks show up within the Rayleigh signal.

Another important aspect of the molecular filter is the preservation of information. By using a photon detector which is not sensitive to the frequency of incoming photons e.g. a CCD camera, an unfiltered image would only hold information on the prevailing density of the molecular ensemble and would lose any information about pressure, temperature and flow velocity. This is due to the fact, that the camera only measures the number of incom-

ing photons, therefore it is not possible to reconstruct the spectral shape of the Rayleigh signal, from which the said properties of the ensemble can be deducted. But if the Rayleigh signal is convoluted with the spectral transmission shape of the molecular filter, the Rayleigh scattering's spectral shape of the signal can be reconstructed.
After the molecular filter has absorbed the unwanted signals in the same frequency range as the Rayleigh signal, an interference filter blocks the signal of all other stray light sources, as will be further discussed in chapter 2.4. A camera then measures the residual light as displayed in figure 6 and yields an intensity value per sensor element. iodine

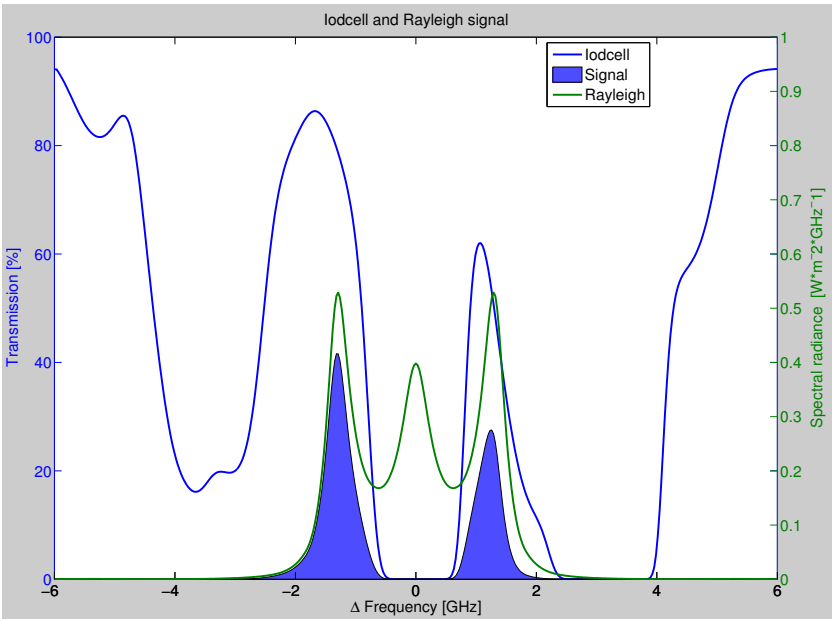

Figure 6: Plot of the Rayleigh signal (green), the transmission profile of an iodine molecular filter with saturation temperature of 70°C (blue) and the resulting signal area (blue area). An integral of the blue marked signal area represents the intensity value taken by the camera.

2.3.2 Mathematical description

The FRS signal is mathematically described as the convolution of the Rayleigh signal r with the absorption spectrum τ of the molecular filter:

$$\sigma_{FRS} = \sigma \int_{\infty}^{\infty} r(x,y) * \tau(\nu + \Delta\nu) d\nu \tag{5}$$

σ is the Rayleigh cross section of the illuminated gas, x and y are the parameters as given in chapter 2.2. Therefore the resulting grayscale intensity

for each separate camera pixel is given by [Dol16]

$$\begin{aligned} S(x,y) =& R(I_0)\Big(n \cdot \sigma_{FRS}(x,y) + ... \\ &+ B_0(I_0)\tau(\nu_0) + B\tau(\nu_0 + \Delta\nu) + C_t\Big) + C \end{aligned} \tag{6}$$

The total intensity can be split up in five main parts. The first part within the brackets represents the FRS intensity. It is the product of n, the particle density, and the modified Rayleigh cross section σ_{FRS} from equation 5.
The second term $B_0(I_0)\tau(\nu_0)$ is a narrowband elastic stray light contribution. It consists of the residual light from Mie- or geometrical scattering, which passed the molecular filter and reached the detector nevertheless. The third term $B\tau(\nu_0+\Delta\nu)$ is similar to the second and is a contribution also based on Mie-scattering processes. However, this term treats the influences of particles moving through the measured area, and therefore their signals are Doppler-shifted. This contribution can render measurements in environments with a high flow velocity useless, if the molecular absorption at the Doppler-shifted frequency is not strong enough.
The forth term C_t describes background influences which emerge as the scattered signal light passes through the detector optic. Since many components within the camera setup own glass surfaces, the signal light is scattered within this setup and sum up to a background signal.
These first four contributions to the total intensity are multiplied with an experimental parameter $R(I_0)$. It may be seen as an efficiency factor of the optical setup and needs to be determined experimentally.
The fifth term C is a background parameter for all influences not covered by the previous, for example ceiling light, the offset of the camera or flame luminosity.

2.3.3 Frequency scanning method (FSM)

The frequency of the generating laser light may be tuned to produce a series of intensity values, since the Rayleigh scattered light's spectral profile stays the same if the mean flow field parameters pressure p, Temperature T and Doppler-shift due to flow velocity $d\nu$ are held constant throughout the measurement (as shown in figure 7) which was firstly presented by Forkey [Fork96]. This is a necessary condition for this procedure, because this method can only derive mean values for these parameters. If the frequency is tuned, the spectrally insensitive camera will measure one intensity value for every frequency as shown in figure 8. This intensity value can be lead

back to the convolution of the Rayleigh signal with the unique transmission shape of the molecular filter among other terms. Therefore the curve of the intensity values gained with the FSM (see figure 8) holds information about all flow field parameters p, T and $d\nu$.

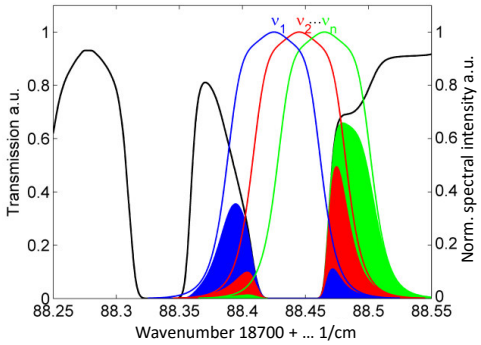

Figure 7: Illustration of the Frequency Scanning Method (FSM). The laser frequency is tuned through the transmission minimum of the molecular filter. For each measurement a different intensity value is received and therefore the accuracy of the procedure is improved equivalently. [Dol16]

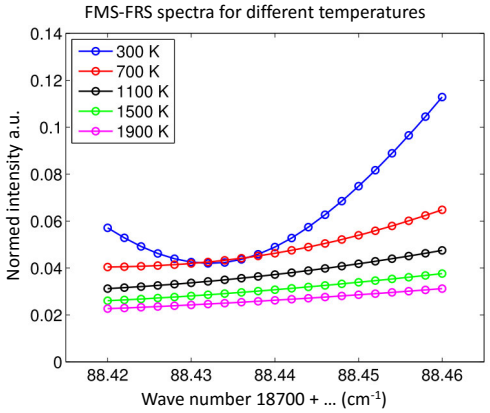

Figure 8: Theoretical intensity values a camera would yield using the Frequency Scanning Method (FSM). Every data point in this plot represents a theoretical convolution of the Rayleigh scattered light's spectrum with the molecular filter (integral over the marked area in the left image). [Dol16]

It is in principle possible by using this measurement method to determine even the calibration parameters R, B_0, B, C_t and C as well, so that equation 6 can be fully solved. The idea of FSM is to take enough measurements at different laser frequencies to have an overdetermined system of equations. Since all the parameters from equation 6 change the shape and/or amplitude of the Rayleigh signal in a distinct way, a theoretical spectrum can be numerically fitted using a Levenberg-Marquardt-algorithm [Vet92] which suites the measurement data best. From this spectrum all calibration parameters as well as the flow field parameters as mentioned can be determined. However if done so, for every parameter which needs to be fitted, the accuracy for each one sinks.

2.3.4 Combined measurement method

To improve the accuracy of the FSM, in this thesis a combined measurement method will be used, which is presented in [Dol16]. The principle of which is to reduce the number of unknown parameters and use the FSM to determine the residual parameters with high accuracy.
The B and B_0 parameters are preferably disregarded, so all Mie-scattered light needs to be absorbed by the molecular filter. Therefore all following FRS measurements will be taken at strong absorption lines of the molecular filter. A background image will be taken to compensate for any constant background signals and will be subtracted from any signal image, therefore C can be removed from the equation. Since the intensity value resulting from C_t emerges as the light travels through the detector optics, and R is also dependent on the distribution of the light intensity, they stay in the equation. Therefore the signal intensities at the different frequencies f are composed of following terms:

$$S_f(R, T, p, d\nu) = R(I_0)\,(n \cdot \sigma_{FRS,f}(T, p, d\nu)_f + C_t) \tag{7}$$

In this combined method any signal levels measured are divided by the arithmetic median of the whole measurement series $< S(R, T) >$. Since $R(I_0)$ is only multiplicatively linked to the right hand side term, it drops out but the curve form of the measurement series will stay intact. Therefore the following quotient term for each frequency f is generated:

$$Q_f(T) = \frac{S_f(R, T, p, d\nu)}{< S_f(R, T, p, d\nu) >} = \frac{n \cdot \sigma_{FRS,f}(T, p, d\nu) + C_t}{n \cdot \frac{1}{F} \sum_{f=1}^{F} [\sigma_{FRS,f}(T, p, d\nu)] + C_t} \tag{8}$$

This expression is independent of $R(I_0)$ and by fitting the curvation of the measurement data generated at the different frequencies f, the flow parameters temperature, pressure and Doppler-shift can be evaluated simultaneously.

2.4 Interference filter

Interference filters are created by several stacks of dielectric materials separated by spacer layers as seen in figure 9. The dielectric stacks are alternating layers of low- and high- refraction index materials and have a thickness of $\lambda/4$, with λ being the central wavelength of the filter. So if the incoming light is reflected within this layer, the total phase difference comes to $\lambda/2$

and thereby destructive interference, between the light reflected at the surface of the material and the light reflected within the material, cancels out reflecting light. Thus all incoming light of the central wavelength must be transmitted. The substrates between the dielectric stacks have a thickness of $(n * \lambda)/2$, therefore the phase difference is exactly λ. Because of that, these layers will behave as if they would not exist and are sometimes called "absentee layers". [Thor]

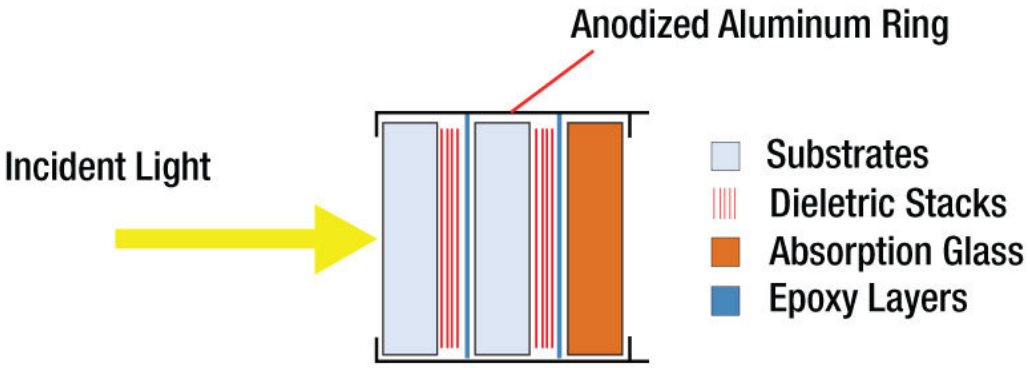

Figure 9: Working principle of an interference bandpass filter [Thor]

Due to this functionality the central wavelength of the filter can be modulated in two ways: Variation of the temperature of the filter or placing the filter under an angle in the light path. Both methods make use of the fact that the layers need to have a specific thickness. As the temperature is raised the materials will expand and therefore the light path within the material lengthens, hence a longer wavelength will be transmitted. This effect is based on the expansion index of the materials and therefore depends on the materials used. To avoid unwanted changes of the central wavelength, the materials are usually thermally very stable. That is why thermal tuning has in general a smaller effect on the central wavelength than the angle tuning method. Using the angle tuning method, the incoming light has to pass the layers at an angle and because of that the effective layer thickness is the original layer thickness divided by the cosine of the incidence angle. Using this modification, the transmitted wavelength can be calculated by the following formula [Yeh88]

$$\lambda(\theta) = \lambda(0)\sqrt{1 - \frac{\sin^2(\theta)}{n_{eff}^2}} \tag{9}$$

Here θ indicates the angle the filter has relative to the incoming light and

n_{eff} is the effective refractive index of the filter, which is unique for each filter design. However, using this method will diffract the light proportional to the angle chosen. This problem can be solved by adapting the camera system to this angle or using a suitable prism.
There are two main reasons why the interference filter is necessary in Filtered Rayleigh Scattering (FRS) experiments. Firstly it is used to suppress a very large part of the black body radiation, as will be described later in chapter 2.5. Secondly it is needed to suppress the luminescence of the molecular filter as it absorbs the scattered light of the laser. This luminescence originates as the green laser light is absorbed by the molecular filter, exciting a higher molecular state. This higher state then decays to a median state and afterwards emits a photon with lower energy as the incoming one to decay to the original state. To prevent the luminescence to contribute to the final signal intensity the interference filter is used.

2.5 Black-body radiation

Everything, whether solid, fluid, plasma or even a large enough amount of gas with a higher temperature than T=0K emits heat radiation. Its intensity, energy and spectral distribution is only depending on temperature. An exceptional position regarding the emittance has the black body emitter. It is known as an object which absorbs any incoming electromagnetic radiation of any wavelength and is therefore an ideal radiator [Mor05]. Hence, it attracted the interest of many physicists. The first theoretical approaches by Wien or Rayleigh and Jeans to describe the mentioned radiation were only valid for limited spectral ranges, up until Max Planck assumed a quantized light field. He postulated a complete theory which is now known as Planck's law [Mor05]:

$$\rho(\lambda, T) = \frac{8\pi hc}{\lambda^5} \frac{1}{e^{\frac{hc}{\lambda k_B T}} - 1} \tag{10}$$

In this equation $\rho(\lambda, T)$ is the energy density dependent on the wavelength λ and Temperature T. This relation is illustrated in figure 10.
To be able to calculate the energy from its density, equation 10 has to be integrated over the wavelength. For the purpos of this thesis however, it is a good enough approximation to use following equation:

$$E(T)\Big|_{\lambda=\lambda_0} = \frac{8\pi hc}{\lambda_0^5} \frac{1}{e^{\frac{hc}{\lambda_0 k_B T}} - 1} \Delta\lambda \tag{11}$$

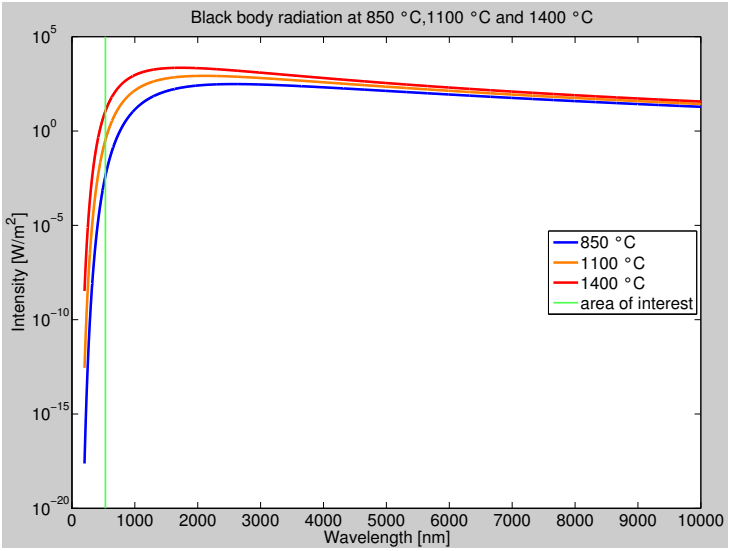

Figure 10: Logarithmic plot of the spectral energy density against the wavelength.

In this equation λ_0 represents the median wavelength in the relevant wavelength range $\Delta\lambda$. This approximation is justified, since an interference filters of bandwidth 0.15 nm is used in the experiments with the Verdi laser and 1 nm in the experiments with the Macropulse system respectively. Therefore the important range is so small that the function is almost constant. In this thesis λ_0 is set to 532.24 nm which is the central wavelength of the frequency doubled Nd:YAG laser system used in the experiments.
In previous measurements it was possible to measure the Rayleigh scattering signal up to temperatures of 850 °C. In this thesis the signal shall stay analyzable in an environment governed by strong thermal radiation up to 1300 °C which corresponds to a 2700 times higher background radiation.
These improvements are especially important for future applications: The vane surfaces in gas power turbines which are right behind the laser beam can reach these levels of temperature and therefore the signal from the background would be much too high to analyze a Rayleigh scattering signal.

3 Experimental setup

In this section some important components of the experimental setup will be described in more detail. The main components are:

1. The laser systems used for the generation of Rayleigh scattered light (chapter 3.1)
2. The camera systems for signal detection (chapter 3.2)
3. The interference filters used for the suppression of stray light and the luminescence of the molecular filter (chapter 3.3)
4. The molecular filter to suppress unwanted contributions from Mie- or geometrical scattering 3.4
5. The wavelength meter used to measure and control the laser system's output frequency (chapter 3.5)
6. The oven to generate blackbody radiation (chapter 3.6)

3.1 Laser systems

In the experiments three different laser systems were used: *Torus*, the *Macropulse* system and *Verdi*. *Torus* was only used for preliminary tests, the *Macropulse* system was used for FRS measurements with the temporal filtering and *Verdi* for FRS measurements with strong spectral filtering.

3.1.1 Torus

Table 1: Properties

Power	50 - 400 mW
Wavelength	532 nm
Spectral Bandwidth	< 5 MHz
Coherence length	> 100 m
Spatial Mode	TEM00
Laser beam quality	$M^2 \leq 1.1$
Beam diameter	1.7 ± 0.2 mm
Polarisation ratio	$> 100 : 1$
Dimension (LxBxH)	18 x 11 x 6 cm^3

The *Torus* laser system by *Polytec* as seen in figure 11 was used for preliminary tests only. It is a continuous wave, frequency doubled Nd-YAG laser with an exiting wavelength of 532 nm. Further technical properties are given on the left side. Its specialty is that it is an actively locked single longitudinal mode laser. The laser uses intelligent

electronics to continually tracks its longitudinal mode position and ensures there is no mode-hop.

Figure 11: Photography of the *Torus* laser system.

3.1.2 Macropulse system

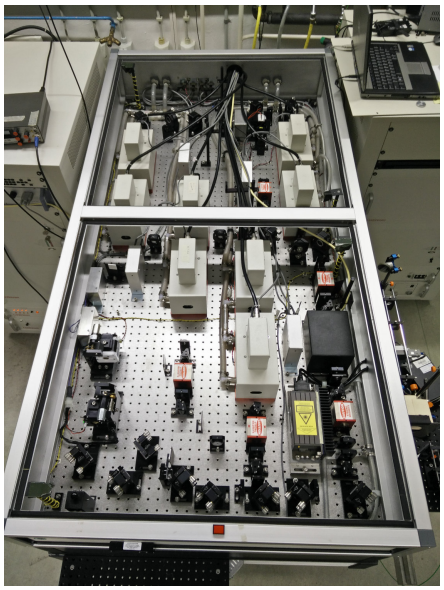

Figure 12: Photography of the Macropulse system.

To filter the background by short exposure times, a long pulse laser system is used as can be seen to the left in figure 12. Its pulses are generated using following principle (figure 13): The continuous wave seed laser with gain medium Nd:YAG emits infrared light (1064nm) which firstly enters a Pockels cell. In this cell the polarization of the incoming beam is rotated every 25 ms for a selectable duration of 1 up to 10 μs. Afterwards all light is deflected by a polarization-selective beam splitter except if the polarization was rotated by the Pockels cell. This procedure creates 1 to 10 μs long laser pulses every 25 ms from the cw laser light. The deflected light is almost

continuous except from the pulses and is decoupled from the Macropulse system, where it can be used to determine the actual wavelength of the system.

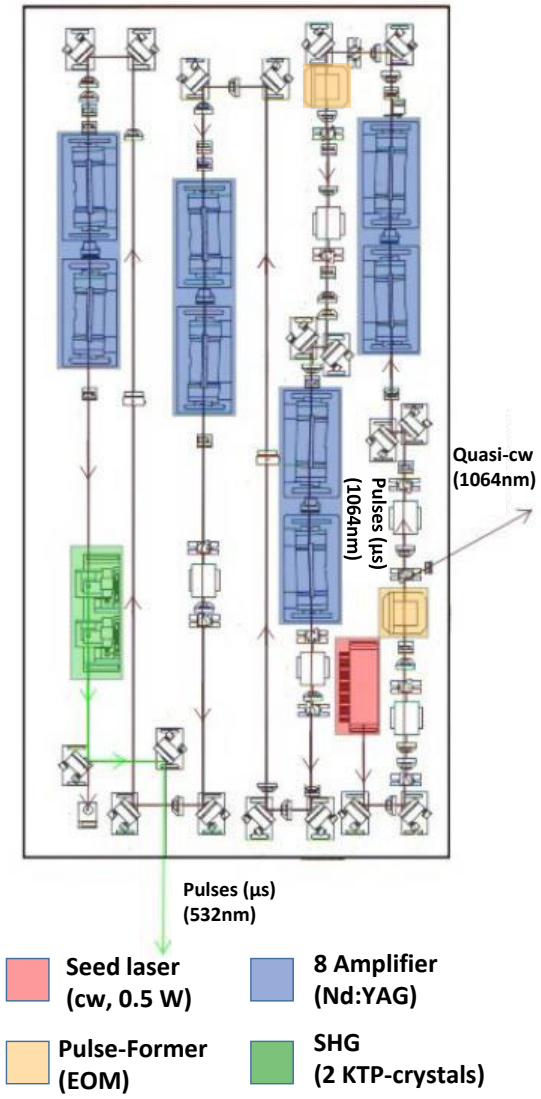

Figure 13: Schematic view of the Macropulse system. The laser light from the Nd:YAG cw seed laser (1064nm) is formed to pulses using an electro-optical modulator. Every pulse is boosted by eight amplifiers. To gain the wanted wavelength of 532 nm, the pulses are frequency doubled by two KTP-crystals. It is possible to use the decoupled light which is not shaped to pulses, to determine the wavelength of the system.

Table 2: Properties

Pulse energy	up to 250 mJ
Pulse rate	40 Hz
Pulse length	1 to 10 μs
Wavelength	532 nm
Spectral Bandwidth	$<$ 1 MHz
Beam diameter	6 mm
Beam divergence	$<$ 1 mrad
Shot to shot stability	$<$ 1 % RMS

These generated seed pulses then pass through eight Nd:YAG amplifier stages which are pumped with flash lamps. Due to this pumping, a population inversion is created which allows the beam to be amplified via stimulated emission. Between the first two amplification stages another Pockels cell is employed to suppress any cw radiation, "leaking" through the pulse shaping electro-optical modulator. After the amplification the laser beam is frequency doubled in two KTP-crystals to become the exiting wavelength of 532 nm. The green radiation is then deflected out of the laser using a frequency-selective mirror and the unconverted 1064 nm radiation is dumped in a water cooled beam dump.
Five Faraday isolators are installed in the system to suppress amplified spontaneous emission within the laser: Two - seperating the seed laser from the amplification stages and three - between amplification stages.
Due to the fact that the seed laser light is amplified in laser-active materials, further resonators are not needed. Therefore a weaker but more frequency stable seed laser can be used, which emits single-mode radiation in TEM_{00}-mode. Due to the usage of this short resonator of the seed laser in comparison to other pulsed lasers, the system is very frequency stable at a low spectral bandwidth of less than 1 MHz.
Another advantage is that the amplification does not happen in the resonators as rather in the amplification stages which reduces the bandwidth of the laser compared to other powerful, frequency stable lasers.
The gain medium's amplification improves with higher frequencies of the seed laser. Therefore it is generally beneficial to use this Macropulse system at the highest frequencies the seed laser is capable of. If done so, the highest achievable pulse energies with this system are up to 250 mJ.

3.1.3 Verdi

The *Verdi* laser system by *Coherent* is a continuous wave DPSS (diode-pumped solid-state) laser. It is used to test the second variant to suppress background radiation by using a spectrally narrow interference filter (see section 2.4). Its gain medium is a $Nd^{3+} : YVO_4$ crystal and is end pumped by the diode-laser beam, which is transported to the head through the fiber optic cable. The LBO crystal frequency doubles the infrared (1064 nm) intracavity

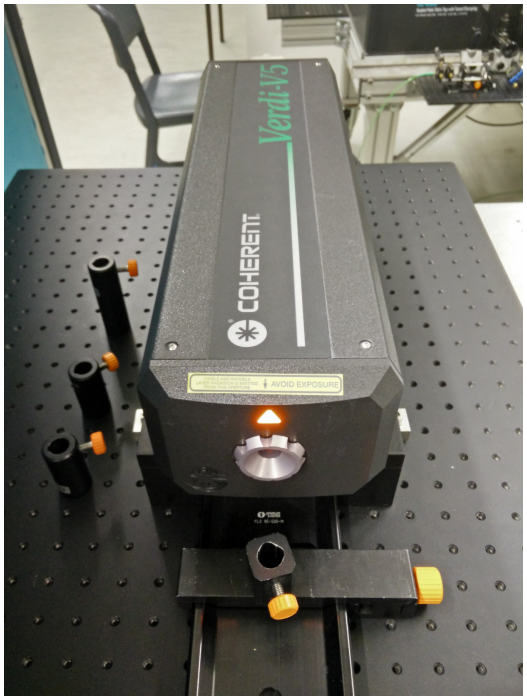

Figure 14: Photography of the *Verdi* laser system.

Table 3: Properties

Power	up to 5 W
Wavelength	532 nm
Spectral Bandwidth	< 5 MHz
Beam Divergence	< 0.5 mrad
Laser beam quality	$M^2 \leq 1.1$
Beam diameter	2.25 ± 10 %
Polarisation ratio	$> 100 : 1$
Power stability	± 1 %
Dimension (LxBxH)	47 x 14 x 11 cm^3

beam generated by the vanadate crystal to produce the green (532 nm) output beam. It provides high-power, mode-hop-free, single-longitudinal-mode output with low intensity noise and a narrow spectral linewidth.
The laser's frequency may be tuned in three different ways so that it has an effective frequency range of approximately 60 GHz. To change its frequency over a large range, *Verdi* has a heatable etalon inserted in the cavity of the laser. This procedure is the slowest way to modulate the frequency since it is necessary to wait for the etalon to be stabilized at the defined temperature, but changes the frequency the most. Another method to almost instantly change the frequency is offered by two piezoelectric elements. They use high voltage of 0 to 100 Volts to modify the length of the resonators. Both piezoelectric elements together may change the frequency in a range of 15 GHz. Due to the frequency stability and its fast tuneability, this laser system is an excellent candidate for fast and reliable FRS measurements with the frequency scanning method.

3.2 Camera systems

For the experiments two different cameras were used, a *Neo* S-CMOS camera by *Andor* and an *ImagEM* EM-CCD camera by *Hamamatsu*. Both cameras were operated using a LabVIEW programs (further information to the pro-

gramming in chapter A.1).

3.2.1 Andor Neo (S-CMOS)

The *Neo* S-CMOS camera by *Andor* as seen in figure 15 is vacuum cooled to $-30°C$ and has therefore good specifications regarding linearity of gray scale intensity to the incoming light intensity (This linearity was checked in chapter 4.2) as well as high sensitivity and a fast readout rate (details seen in table 4). It was the camera of choice for measurements with the Macropulse system. With this camera system every pulse of the Macropulse system could be measured and evaluated separately.

Table 4: Properties

Active Pixels:	2560 x 2160 (5.5 Megapixels)
Sensor size:	16.6 x 14.0 mm (21.8 mm diagonal)
Pixel size:	6.5 μm
Pixel readout rate:	200 MHz or 560 MHz
Minimal exposure time	(global shutter mode) 10 μs
Read noise Median [rms]	$< 2.5\ e^-$
Minimum air cooling temp.:	$-30°C$
Maximum burst frame rate:	100 fps at full frame
Data range:	12 or 16-bit
Linearity (in %, maximum):	Better than 99%
Binning:	2x2, 3x3, 4x4, 8x8
Trigger modes:	Internal, External, External Start, External Exposure, Software Trigger

In the later discussed FRS experiments (chapter 4.4) the camera is triggered by the time control unit of the Macropulse system to start an acquisition of 50 images with an exposure time of only 30 μs, therefore another advantage is the minimal exposure time of only 10 μs. This is crucial for such measurements with high black body radiation, because therefore the camera chip may only be exposed as long as the laser pulse is present, to minimize the error signal from this contribution. The 30 μs were chosen to be completely sure to have the laser pulse within this time window.

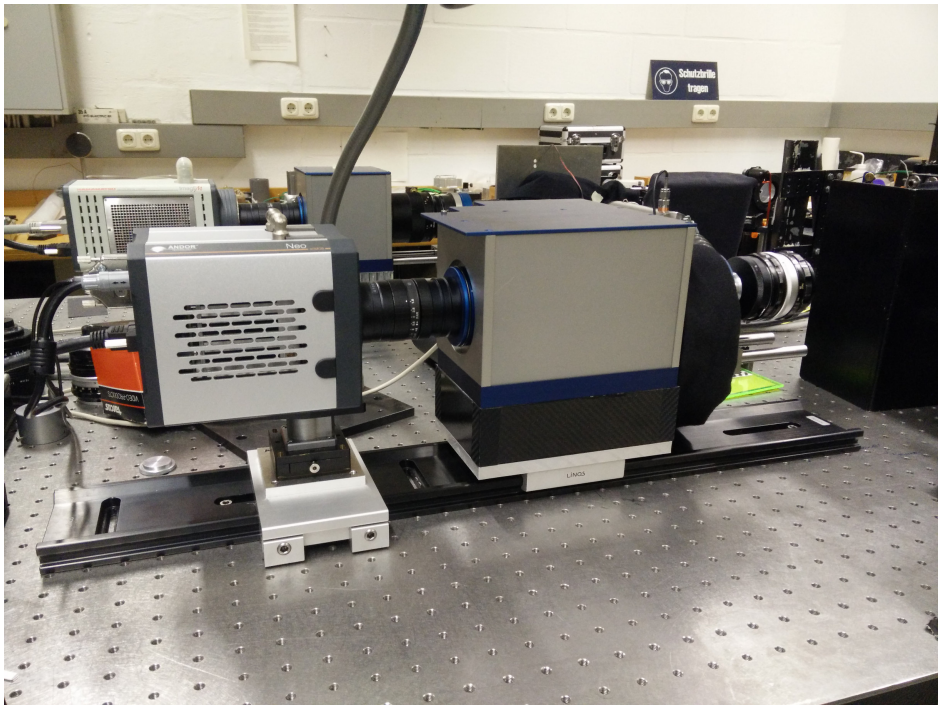

Figure 15: Photography of the Camera system with *Andor's* S-CMOS *Neo* camera on the left.

In comparison to FRS measurements with a cw laser source in which the camera chip has to be exposed for several seconds, the camera only captures a fraction of the black body radiation.

3.2.2 Hamamatsu ImagEM (EM-CCD)

The *ImagEM* by *Hamamatsu* as seen in figure 16 is a back-illuminated electron multiplying CCD camera, which may be used in an amplifying EM- or normal CCD mode. It has a very high quantum efficiency of over 90% at the required wavelength of 532 nm. Due to its stable air cooling performance, the camera may be used at -65 °C. Therefore the dark current is minimized at 0.01 e^-/pixel/s and allows low noise FRS measurements. In addition to that the camera was used in the normal CCD mode for all following FRS experiments, since the EM magnification of the signal would have caused additional noise. However this characteristic may differ in extremely low signal intensity regions.

Table 5: Properties

Active Pixels:	512 x 512 (0.26 Megapixels)
Sensor size:	8.19 x 8.19 mm (11.6 mm diagonal)
Pixel size:	16 μm
Minimal exposure time:	(externally triggered) 10 μs
	(internal sync mode) 30.5 ms
Read noise Median [rms]:	$< 17\ e^-$
Dark current:	0.01 e^-/pixel/s
Minimum air cooling temp.:	$-65°$C
Maximum frame rate:	31.9 fps at full frame
Data range:	16-bit
Binning:	2x2, 4x4
Quantum efficiency at 532 nm:	$> 90\%$

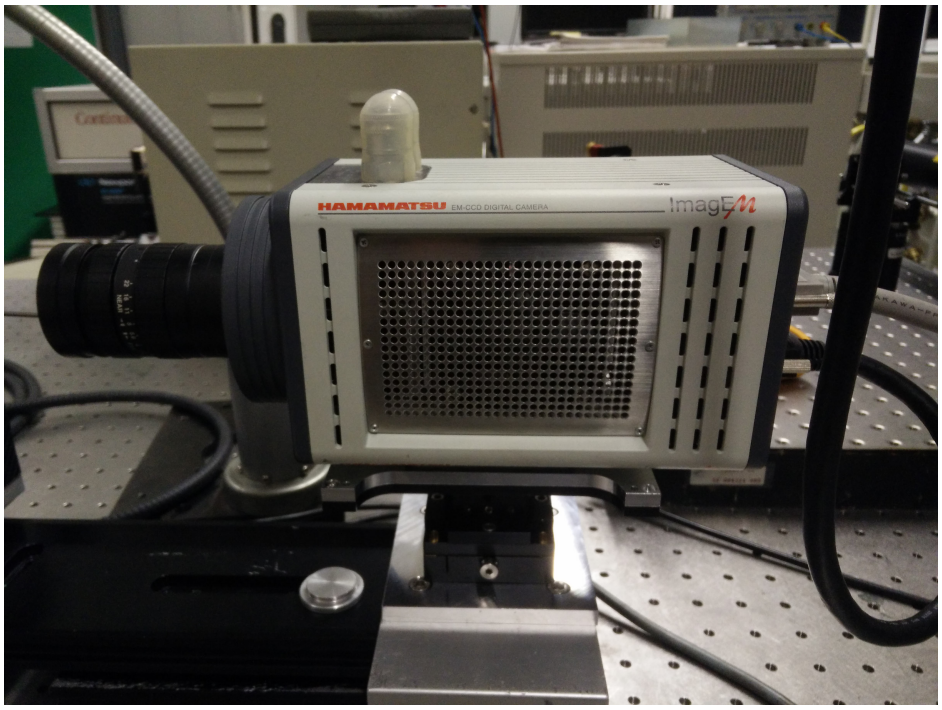

Figure 16: Photography of *Hamamatsu's ImagEM*

3.3 Interference filter

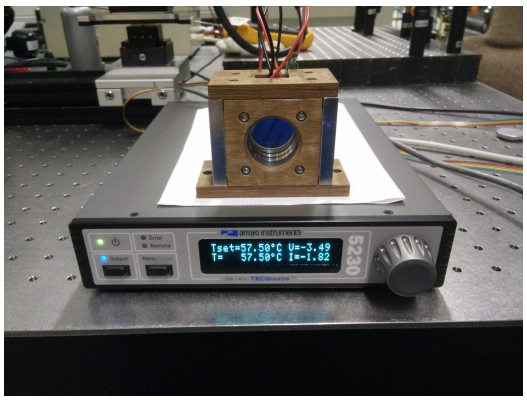

Figure 17: Photography of the 0.15 nm Interference filter by *Alluxa* in its thermal stable housing. Below is the TEC controller regulating two Peltier elements to the left and the right of the filter within the housing.

For this thesis two different interference filters were used, a flat top interference filter by *Barr* with a bandwidth of 1 nm (see figure 18) and a Lorentz shaped interference filter by *Alluxa* with a FWHM of 0.15 nm (see figure 19). Due to the extreme thin FWHM and the Lorentz profile of the Alluxa filter, it has to be thermally as stable as possible to guarantee a constant transmission percentage throughout the frequency scanning in the FRS measurements. Therefore a special housing was designed and built as can be seen in figure 17. It has two peltier elements to the left and the right of the filter which keep the temperature stable down to 10 mK at a set point from room temperature up to 80 °C.

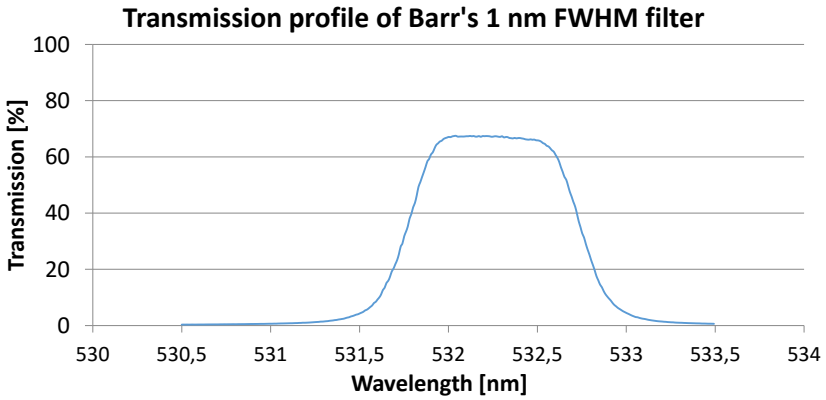

Figure 18: Theoretical transmission profile of *Barr's* 1 nm FWHM interference filter with central wave length of 532.24 nm.

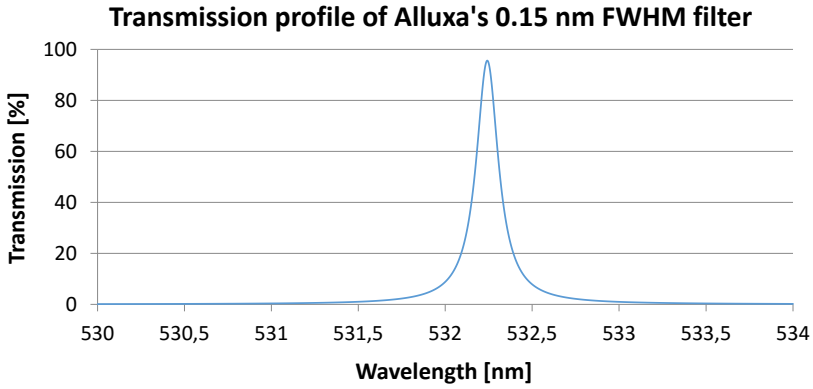

Figure 19: Theoretical transmission profile of *Alluxa's* 0.15 nm FWHM interference filter with central wave length of 532.24 nm.

With this temperature controlled environment, it was possible to shift the transmission band of the interference filter to contain the FRS measurement's frequency range. Chapter 4.5 explains the experiments done to determine the exact temperature.

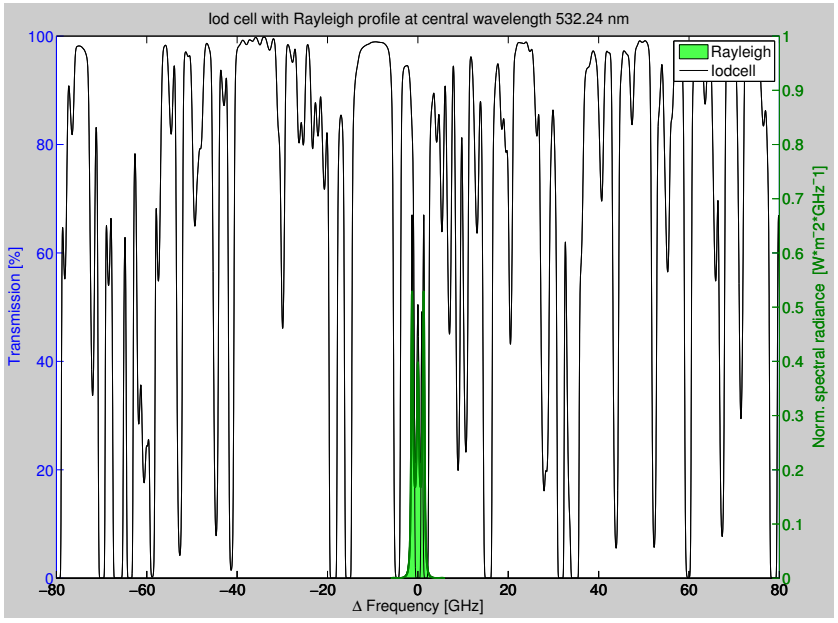

Figure 20: The Rayleigh-scattering profile set into perspective to the FWHM of the 0.15 nm bandpass filter ($\approx$ 160 GHz). The black line indicates the transmission spectrum of a molecular filter (iodine) with saturation temperature of 70°C

Even though *Alluxa's* interference filter is one of the narrowest bandpass filters commercially available, which is not a combination of an interference filter and an etalon, the spectal region cut out with this filter ($\approx$ 160 GHz) is still very large in comparison with the spectral bandwidth of the Rayleigh signal of a few GHz (see figure 20).

3.4 Iodine as molecular filter

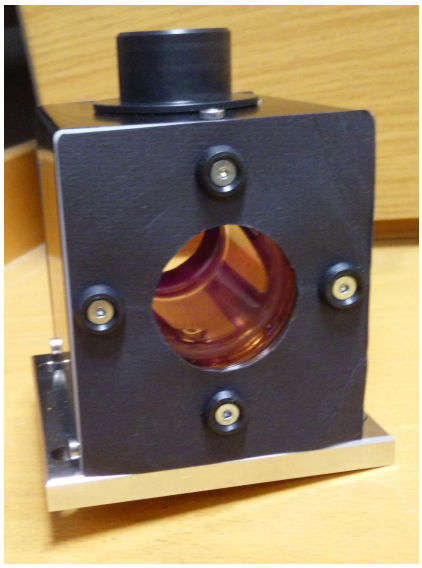

Figure 21: Photography of the iodine cell. It consists of a glass cylinder containing the iodine, which is surrounded by a thermal housing. The housing is heated 10 degrees further than the necessary saturation temperature and is thermally isolated.

The center of the camera system builds the molecular filter (see figure 21). A specific amount of iodine is enclosed in an evacuated glass cylinder. The quantity of the iodine enclosed determines the necessary saturation temperature of the cell, so that all iodine is gaseous. If heated beyond this temperature, the absorption will only be modified by minor pressure dependent influences. Therefore to ensure that all iodine is at all time gaseous, the cells are always heated to 10 degrees more than the marked saturation temperature. Due to Beer's law the light intensity I weakens proportional to following formula [Gun03]:

$$I = I_0 \cdot 10^{-\epsilon c l} \tag{12}$$

I_0 is the intensity before the light passes through the iodine cell, ϵ is the molar attenuation coefficient, c is the amount concentration and l is the path length the light has to pass through the material.

To prevent interference patterns emerging from the cell's entry and exit windows the glass cylinder had angled windows as well as an anti-reflection coating for green light. For later experiments the iodine cell with 70 °C saturation temperature with AR coating and angled windows was used. The exact spectral transmission shape of this iodine cell was also measured in chapter 4.3.

3.5 Wavelength meter

Figure 22: Photography of the wavelength meter on the left as well as the measureing card on the right. It is connecting the computer to the other experiment components like the temperature controller of the Macropulse's seed laser or the slow entry of the Verdi laser.

In FRS, the laser's output frequency has to be precisely known, therefore a *WSU-10* by *HighFinesse* as seen in figure 22 was used. It can measure the wavelength of visible light down to 10 MHz accuracy. In order to keep this precision throughout long measurements, the wavelength meter has to be recalibrated every 5 minutes to a reference source (here a HeNe-laser). The wavelength meter itself has a -4 to 4 Volts exit to stabilize a laser directly using its implemented PID-controller. This feature was utilized to stabilize the Verdi laser as well as the seed laser of the Macropulse system by controlling the piezoelectric elements within the laser. If the control parameters are set correctly for each individual laser, a constant frequency stability of only a few MHz can be achieved. The wavelength meter works on the basis of a Fizeau interferometer. The beam enters the optical unit via a fiber, is collimated by a lens and then split into several beams. Each beam passes a Fizeau interferometer of specific length to generate distinct interferometric patterns. All these patterns are recorded by a CCD array and digitally transferred via USB interface to the operators PC. The firmware finally analyses the data and calculates the laser wavelength, taking into account the ambient temperature [Top]. Also the wavelength meter may be addressed using a LabVIEW program which speeds up the FSM. Further details are given in chapter A.1.

3.6 Oven

To have similar thermal conditions as in a gas power station, an oven was used. An overview is shown in figure 23 and a view through the oven in figure 24. It consists of an insulating casing and heats the empty space inside via heating coils. It is designed to approximately increase the temperature to 100 times the applied voltage in °C. The highest temperature reachable with this device is 1175 °C. Since the oven is missing a temperature stabilization unit, the temperature has to be maintained manually by adjusting the supply voltage. Due to this fact, the temperature measured with the thermocouple varied around the set temperature with an amplitude of ±5 °C. To be able to tell the temperature during the experiment as precise as possible the thermometer was placed only a few millimeters away from the the laser beam.

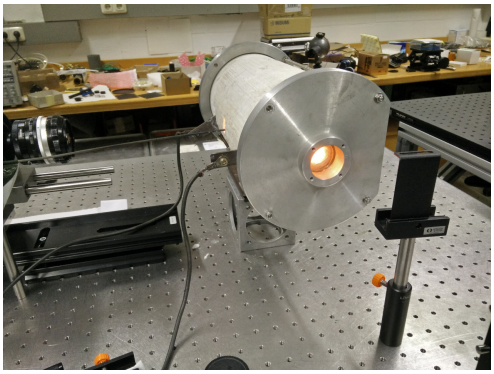

Figure 23: To 1000 °C heated oven from the side. The black body radiation is so intense that a photo through the oven would be overexposed.

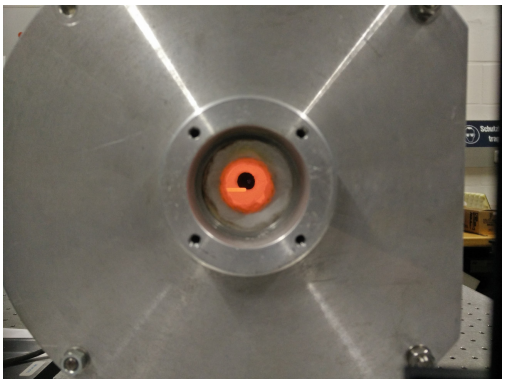

Figure 24: To 600 °C heated oven viewed inside with the hot thermometer tip visible only millimeters away from where the beam path will be.

4 Experiments

4.1 Analysis of different interference filter positions

In this experiment different configurations of camera lenses and interference filter positions were tested to achieve highest transmission and weak interference patterns, due to the filter.
Since the filter produces an interference pattern if it is placed in a collimated light path two alternative positions were tested. The first had a slightly divergent beam path to suppress interference effects and the second used a telecentric light path. The latter solution uses a set of two additional camera lenses to create an intermediate image in which the filter is placed. Since here the light is not parallel, no interference patterns should emerge.

4.1.1 Setup

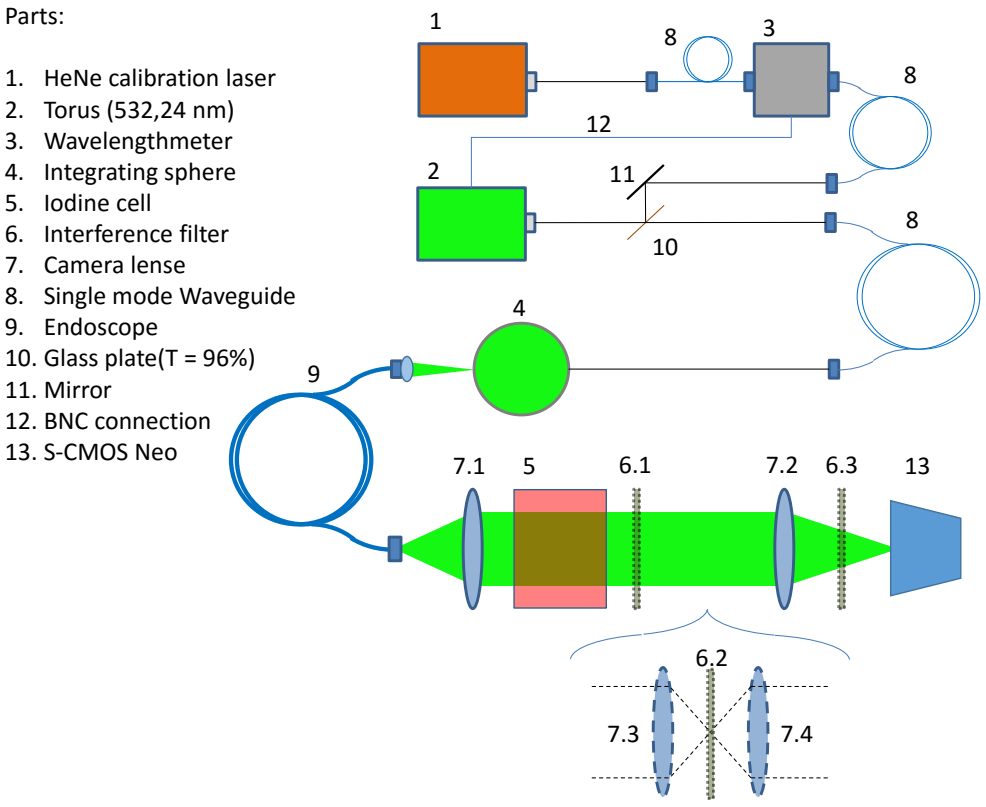

Figure 25: Setup to find the best possible position for the interference filter in the camera system

In this setup the wavelength meter (3) was calibrated by a Helium-Neon-laser (1) and measured the wavelength of the *Torus* (2) laser. A part of the laser beam was deflected via a glass plate (10). The rest of the beam was guided by an optical fiber (8) to the integrating sphere (4) illuminating a circular area of 4 cm in diameter homogeneously. An endoscope (9) transferred the image of the integrating sphere's exit to the camera system. It consisted of a retro-oriented camera lens (7.1) with a focal length of 35 mm, the iodine cell (5), another forward-oriented camera lens (7.2) with focal length of 100 mm and *Andor's* S-CMOS Neo camera (13). This setup produced almost a tripple magnification and therefore the camera chip the size of 16.6 mm x 14.0 mm was well illuminated by the exit of the endoscope the size of 4.0 mm x 4.0 mm. An *Andover* interference filter with 3 nm bandwidth was tested at position 6.1 (parallel light path), 6.2 (telecentric light path) and 6.3 (slightly divergent light path). Also a *Barr* interference filter with 1 nm bandwidth was tested at position 6.2 to show the strong angle dependency. For the telecentric beam path an additional set of two camera lenses (7.3,7.4) with focal lengths of 50 mm was used (The first was forward-oriented, the second retro-oriented).

4.1.2 Results

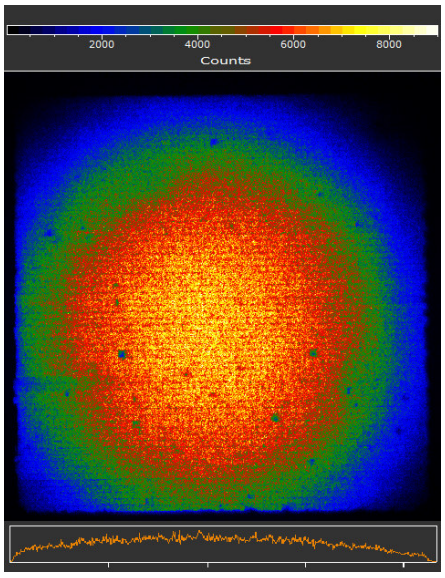

Figure 26:
Reference image without a filter.

All following images were corrected by a background image to subtract influences due to the camera's dark level count as well as background light.
Figure 26 shows a reference image without the filter, to set a maximal limit for the transmission intensity. In figure 27 the filter was placed in the slightly divergent beam path at position 6.3. Here the angle of the incoming light had a good balance to not produce interference rings with good transmission intensity.
Figure 28 shows the resulting image with a completely collimated light path through the filter. In this image the interference rings are clearly visible. However, if the last camera lens was focused slightly and the

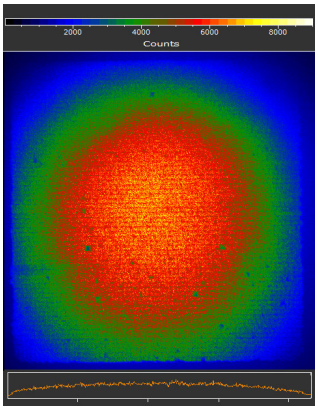

Figure 27:
Image with the filter in between the camera and the last camera lens. (Position 6.3)

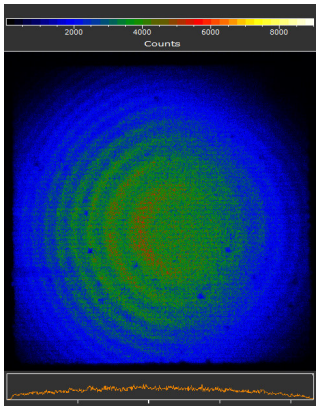

Figure 28:
Image with the filter in the collimated beam path. (Position 6.1)

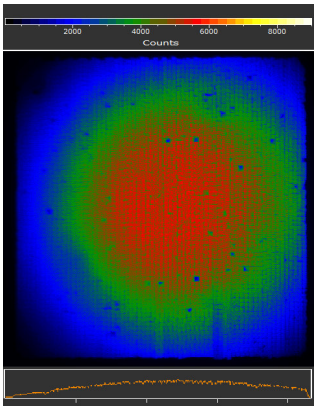

Figure 29:
Image with the filter in in the collimated beam path but slightly focused.(Position 6.1)

camera lens 7.1 was adjusted to get a sharp image, the angle of incidence can be manipulated continuously. Therefore in figure 29 the filter was still at the position 6.1, but the camera lenses 7.1 and 7.2 were slightly focused to suppress the interference pattern.
For the images with the telecentric setting, the scale of the intensity was set to a maximum of 1200 counts instead of 9000 counts in the images before, to be able so see a signal on the images. Therefore the reference image with the telecentric setting (figure 30) seems to have a slightly higher signal maximum than the reference image in the collimated light path, even though the telecentric setting caused a loss of intensity. In Figure 31 the *Andover* filter with FWHM of 3 nm was used and produced a significant loss of intensity. The absorption was even intensified if the *Barr* filter with a FWHM of 1 nm was used as seen in figure 32.

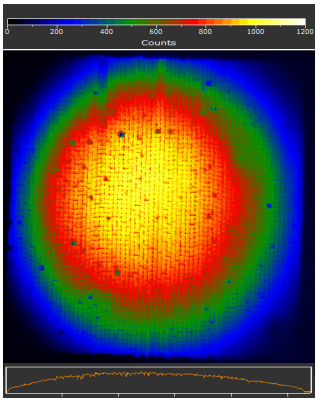

Figure 30:
Reference image with the telecentric beam path configuration without a filter.

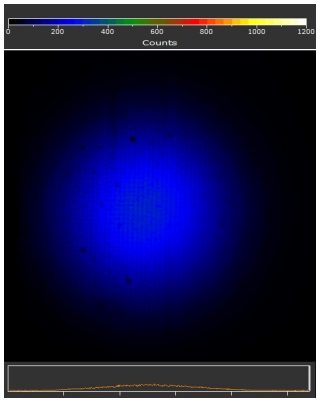

Figure 31:
Image with *Andover's* 3 nm bandpass filter in the telecentric beam path configuration. (Position 6.2)

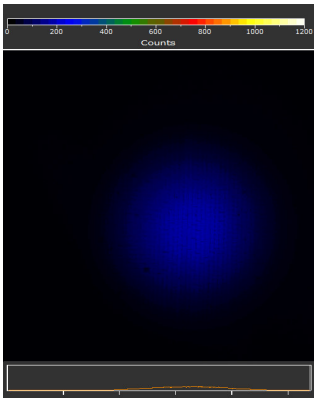

Figure 32:
Image with *Barr's* 1 nm bandpass filter in the telecentric beam path configuration. (Position 6.2)

To set the different settings into perspective, an area of 100 x 100 pixel around the maximal intensity was averaged and is displayed in figure 33.

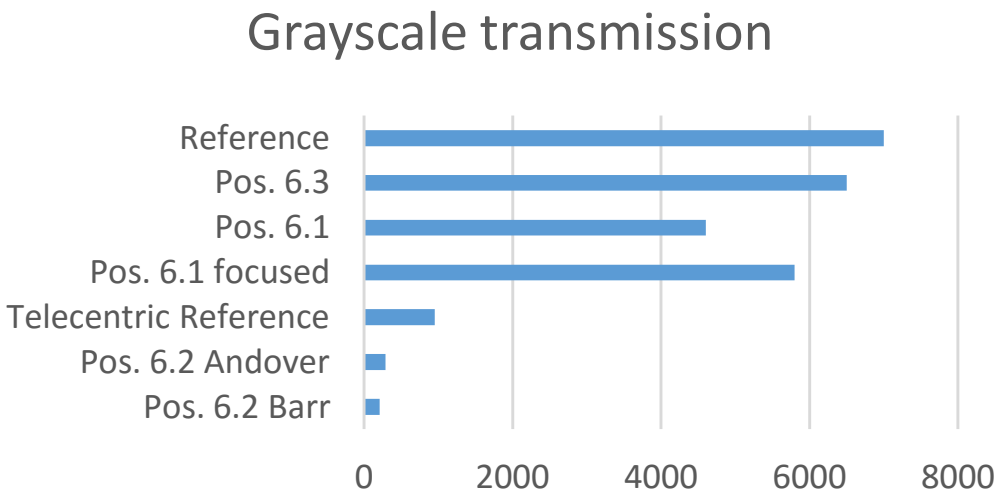

Figure 33: Figure of the transmission change in different configurations. Y-axis labels the Filter position marked in figure 25 and the x-axis shows the grayscale intensity measured with the S-CMOS camera in the regarding configuration.

4.1.3 Conclusion

Due to the major drop of intensity in the telecentric filter setting as visualized in figure 33, this setup was unsuitable for FRS measurements. As for the positions 6.3 and 6.1 with slightly focused lenses, both were acceptable since no interference pattern emerges and the intensity drop is minimal. Although the signal intensity was a little higher if the filter was positioned between the last camera lens and the camera, this position was very unstable since the camera lens and the filter had to be held individually. In the setup 6.1, the filter could be screwed together with the camera lens and the camera, so that no stray light could enter the camera. Therefore the position 6.1 in which the filter is placed before the last camera lens in a slightly focused light path was preferred for the next experiments.

4.2 Analysis of the linearity of Andor's S-CMOS camera

To test *Andor's* S-CMOS camera *Neo* regarding change in exposure time and incoming laser intensity, linearity tests were performed.

4.2.1 Setup

Parts:

1. He-Ne calibration laser
2. Verdi (532.29 nm)
3. Wavelength meter
4. Integrating sphere
5. Camera
6. Camera lens
7. Single mode Waveguide
8. Glass plate (T = 96%)
9. Dielectric mirror (T = 0.4%)
10. BNC connection
11. Diffusing plate
12. Lens (f = 20)
13. Gray filter
14. Diode

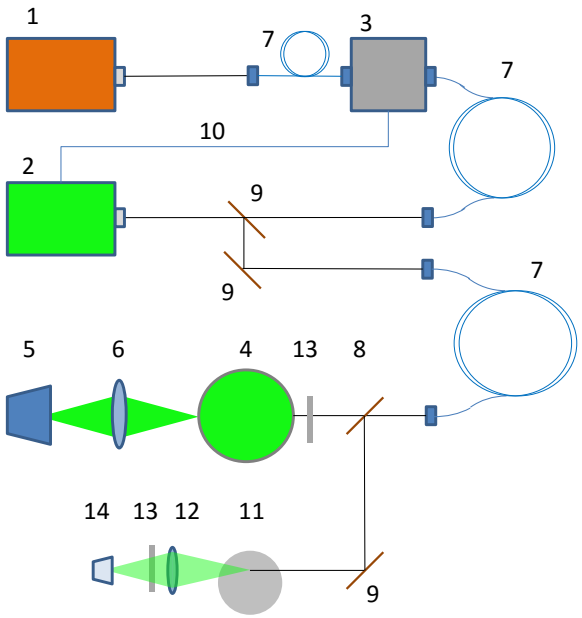

Figure 34: Setup of the linearity tests of the S-CMOS camera

This setup was similar to the setup shown in figure 25, however now the interference filter, the iodine cell and some camera lenses were set aside. For this experiment the laser source was the *Verdi V5* cw-laser instead of the *Torus* laser before. It can produce 5 Watts so that it was not necessary to split off some light with a glass plate for the wavelength meter (3) as before but rather use the 0.4% transmitted through the first dielectric mirror. Since the laser intensity had to be known precisely, a part of the incoming laser beam was split via a glass plate (8) to an intensity measuring unit as follows. After separation, the beam was scattered by a rotating diffusing plate (11) and a part of the scattered light was then focused on the diode (14) by a convex lens with focal length of 20 mm (12). The diffusing plate was included in the intensity determination to prevent interference patterns on the diode which would disturb the measurement while scanning the laser's output frequency. To find the best intensity to not damage the diode but also to have a good signal strength, a suiting gray filter (13) was inserted.
The main part of the beam after the glass plate was then weakened by another set of two gray filters with transitivity $T = 0.05\% * 23\% = 0.0115\%$. Since the laser is unsteadier at lower powers, higher ones are more advantageous. Nevertheless it is necessary to reduce the beam intensity so that the dynamic of the camera was utilized best, therefore gray filters were inserted into the beam path.

4.2.2 Results

In these experiments linearity is tested in terms of incident laser energy on the one hand and camera exposure times on the other, since these dependencies are extremely important for any future measurements. Before this analysis, a background image was taken and subtracted from all measured images with constant binning and exposure time. For this test, the camera was set to global shutter mode at a readout rate of 560 Hz. No binning was used and in the first three measurement series, the exposure time was set to 1 second while the laser power was three times varied from 1 to 5 Watts with 0.1 Watt step size. To evaluate the measured pictures of the three individual rows, an average over an area of 500 x 500 pixel of each one of them was taken as signal value. Afterwards, the values of the three measurement series were averaged as well to minimize the error. To verify the linearity of the camera, these measurements were then fitted with a linear fit in figure 35.

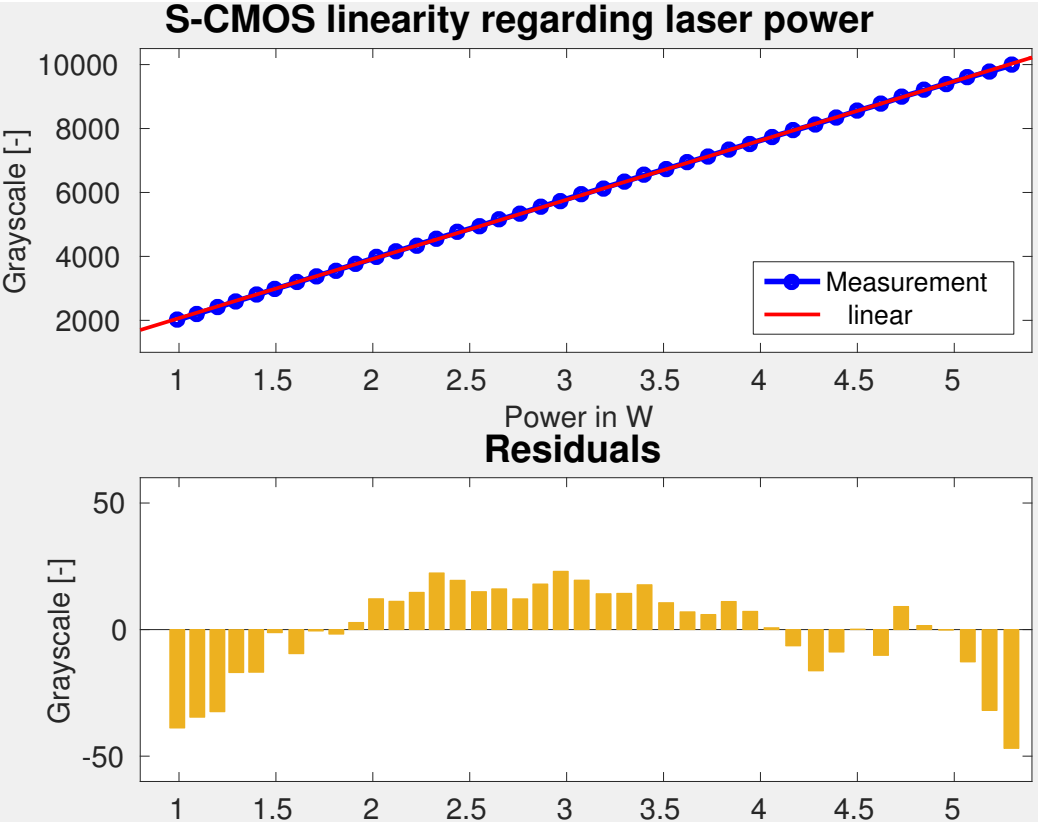

Figure 35: The upper figure visualizes the increase in grayscale intensities measured with the S-CMOS camera against the raise in laser power. Here three series of measurements from 1 to 5 Watts laser power were averaged and then fitted with a linear equation. The lower figure shows how much the individual measurements deviate from the fit in absolute counts.

For the second part of the experiment to evaluate the linearity regarding the exposure time, every measured image was corrected with a background image with the same exposure time. Besides that, a similar procedure was executed to estimate the error made by changing the exposure time. Here the laser power was set to 0.5 Watts and the exposure time was changed in the interval of 1 to 10 seconds in step size 1 second from 1 to 10 seconds. These results were then also fitted with a linear fit in figure 36.

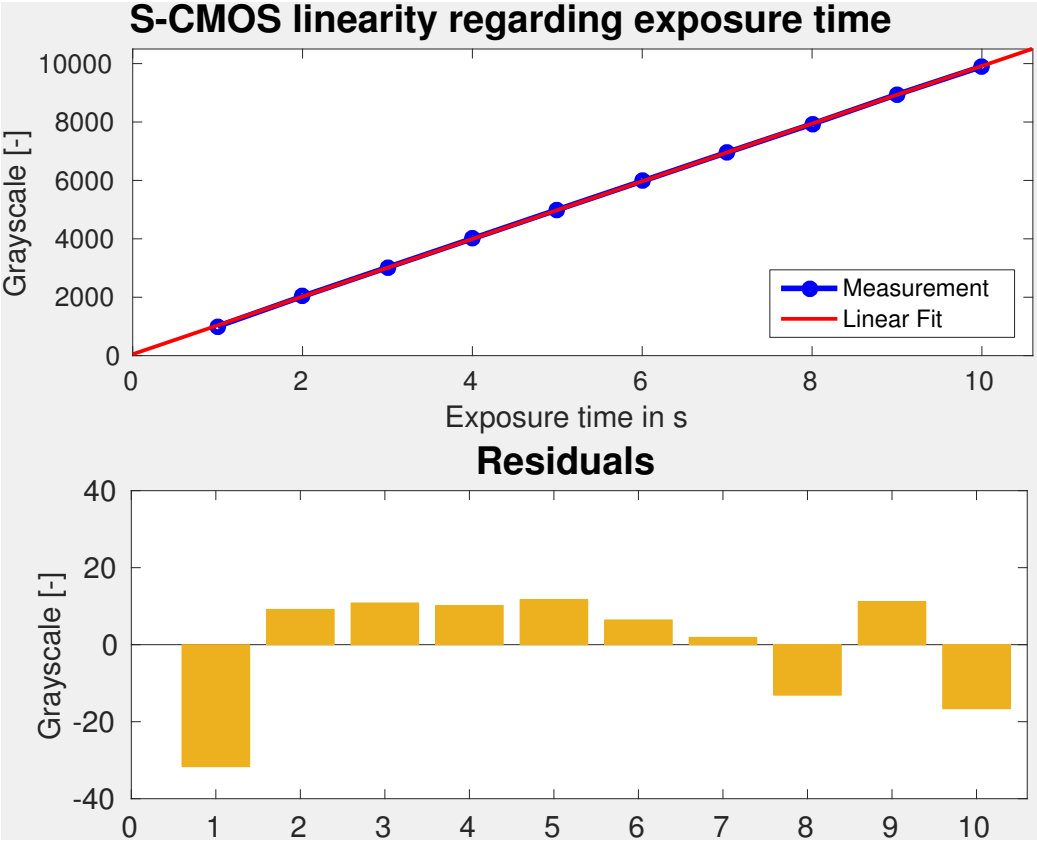

Figure 36: The upper figure visualizes the increase in grayscale intensities measured with the S-CMOS camera against the variation of exposure time. Here three series of measurements from 1 to 10 seconds exposure time were averaged and then fitted with a linear equation. The lower figure shows how much the individual measurements deviate from the fit in absolute counts.

4.2.3 Conclusion

In the figures 35 and 36 the measurement data was fitted with a linear fit. The modulation of the laser power experiment shows that the mean deviation from the linear fit is below 1% of the measured grayscale value if the corresponding grayscale intensity is between 2000 and 10000 counts. The second experiment was performed to test whether the internal timing would also be linear if the camera is exposed to a constant light source. Here the mean deviation is also below 1% of the measured grayscale value. However the linearity regarding exposure times below 1 second as well as intensities below 2000 counts was not checked, so that the camera's linearity is only conclusively proven for measurements with intensities above 2000 counts and

exposure times above 1 second. These conditions are present in FRS measurements with the cw laser source in which the exposure time can be as high as 5 to 20 seconds to have a high enough grayscale intensity.

4.3 Specification of the transmission of the Iodine cell

To calculate the convolution of the Rayleigh scattering signal with the absorption of the iodine spectrum, the latter has to be measured precisely. This spectral integral of the normed Rayleigh signal without a filter is defined to converge exactly to 1, if it is calculated over the whole spectral space. However, the integral's value is still above 0.998 if it is calculated in a range of ± 0.3 wave numbers, hence the error made here is below 2‰ and will therefore be neglected. Since the Macropulse system has a spectral range from approximately 18786.3 cm^{-1} to 18787.9 cm^{-1}, the two strong absorption lines at wave numbers 18786.65 cm^{-1} and 18786.76 cm^{-1} were used for FRS measurements (see figure 37).

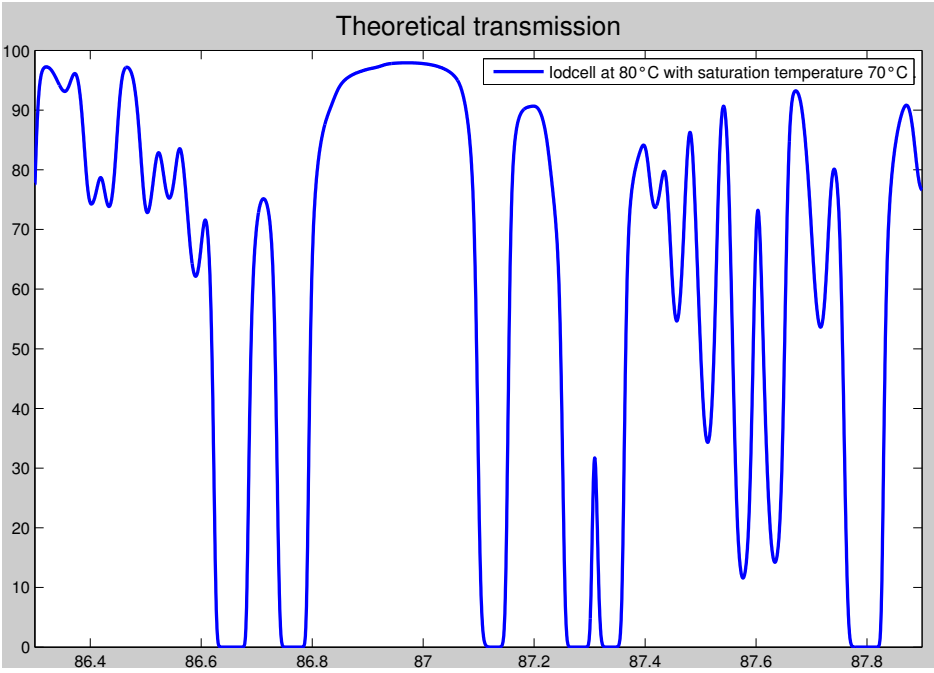

Figure 37: Theoretical transmission pattern calculated with the transmission algorithm by Forkey [For97].

It would have also been possible to use the absorption line at the wave number 18787.8 cm^{-1}, but then a significant part of the Rayleigh spectrum would be left out. Since the convolution integral only converges sufficiently if the

molecular absorption is known ±0.3 wave numbers from the laser's frequency. The contribution from the transmission at 18787.9 cm^{-1} up to 18788.1 cm^{-1} would then not be considered.

4.3.1 Setup

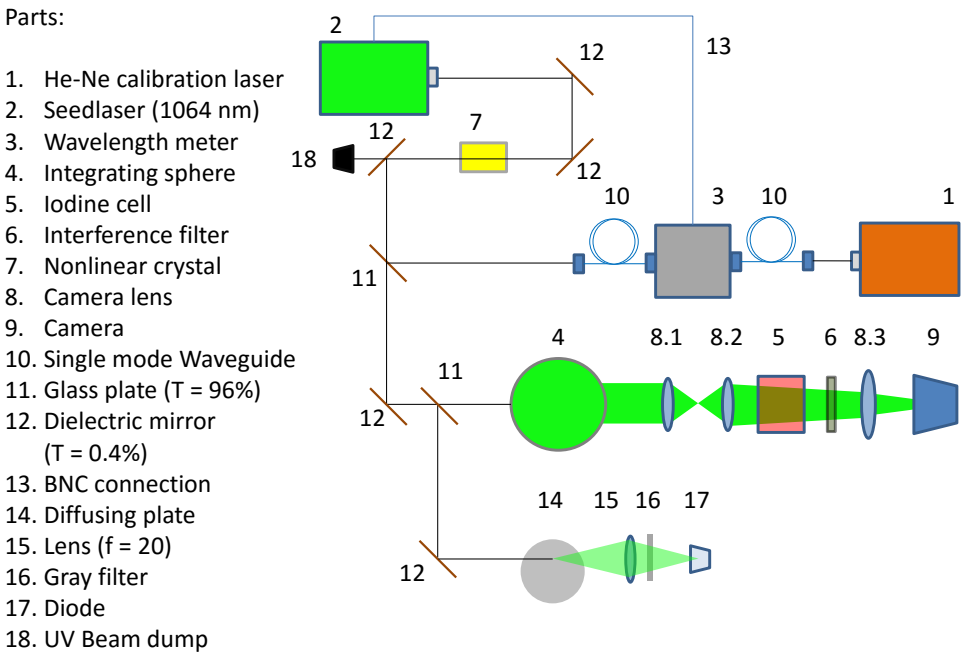

Figure 38: Setup for the specification of the transmission shape of the iodine cell.

This setup is very similar to the one used to determine the linearity of the S-CMOS camera. Here the laser in use is the Seedlaser (2) of the Macropulse system which is frequency doubled by a nonlinear crystal (7) before it is guided to the integrating sphere (4). After that, the light is led through the iodine cell with 70 °C saturation temperature (5) and the interference filter (6) towards the S-CMOS camera (9). The laser intensity is measured by the same diode assembly (components 14-17) which was used in the setup before (chapter 4.2)

4.3.2 Results

In this experiment three series of measurements were performed in which the laser was tuned from 18786.3 cm^{-1} up to 18787.1 cm^{-1} with the step size of 0.002 cm^{-1}. An existing LabView program was modified, to tune the

laser and take an image of the integrating sphere afterwards. To interpret the intensity signal gained by the camera image as a transmission value, the image had to be corrected by subtracting a background image taken without laser light. Afterwards the median value of an area of 100 x 100 pixels in the center of the integrating sphere was taken to average out irregularities at the surface of the integrating sphere. This intensity value was normalized by the laser intensity variation measured with the diode. After that the maximal value of the measurement series was set to 100% transmission. The three measurement series were then merged and compared to a theoretical calculated spectral transmission pattern on the basis of [For97] and displayed in figure 39:

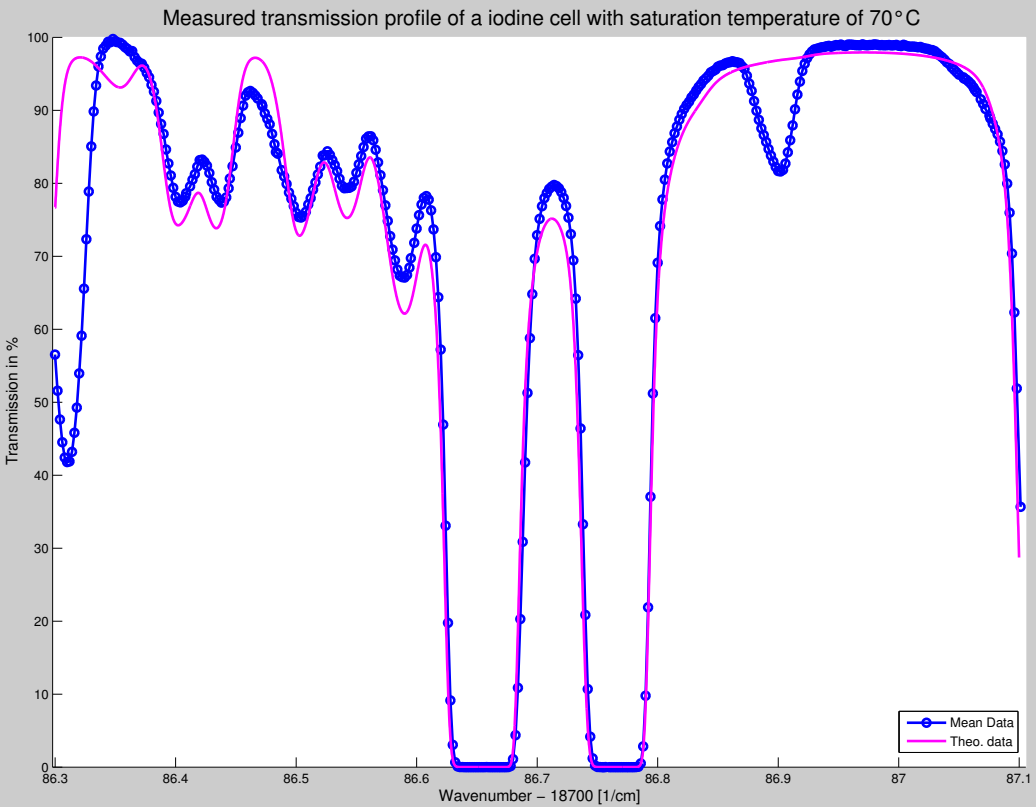

Figure 39: Plot of the merged transmission profile (blue) in comparison to the theoretical data (pink) against the wave number.

4.3.3 Conclusion

The reason why the theoretical transmission data differs from the data set measured here, is that the algorithm uses the measured molecular absorption

lines of iodine molecules as they were measured and catalogued in [Ger79]. From that it calculates the resulting transmission pattern. Hence there are most certainly some lines missing, for example at 18786.88 cm^{-1} it seems like such a case. Also the smaller differences throughout the spectrum may be a result of slightly different line widths of the iodine lines. Since these errors cannot be fully accounted for in the program, this calibration measurement needed to be performed. The measurements deviate from each other below 1% of the measured grayscale value and therefore establish a reliable basis. The transmission spectrum gained here is used in the following chapter to evaluate the convolution between itself and the Rayleigh signal's spectral distribution.

4.4 FRS measurements with the Macropulse system with thermal background

After the preliminary tests, the existing software had to be modified to operate the Macropulse laser system. A basic structure to operate the S-CMOS camera via a LabView GUI was already in place. However the main difficulty was to synchronize the camera with the frequency of the laser pulses as well as a modification of the software to take a series of images, which were then processed and combined. This topic is presented in more detail in the attachment of this work (see chapter A.2).
In this work 50 laser pulses were measured individually with a pulse length of 10 microseconds. To have a signal intensity as high as possible in the camera image, binning was set to 8 and an exposure time of 30 microseconds was chosen. The exposure time was set as short as possible to reduce the influence of the background, but it also needed to be long enough to guarantee the pulse to be within the exposure of the camera chip.
After the modification of the software was finished, a reference measurement at room temperature was taken to verify the functionality of the setup. The next step was to heat the oven to a defined temperature, let it stabilize at the set point and take five series of images at the two absorption lines mentioned in chapter 4.3. As soon as all the data at a set temperature was taken, the acquired intensity spectra were evaluated and the resulting temperature was compared to the temperature measured with a thermocouple.

4.4.1 Setup

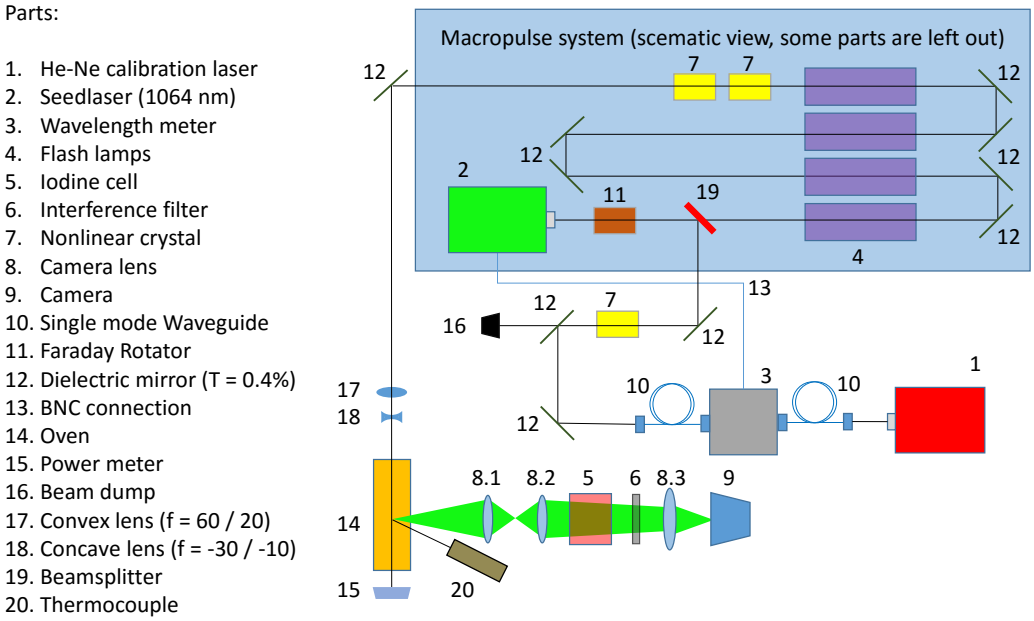

Figure 40: Setup of the FRS measurements with the Macropulse system.

In this setup the deflected cw laser beam of the seedlaser (2) was used for wavelength stabilization. If the Faraday rotator (11) does not rotate the polarization of the laser beam, the light is decoupled from the Macropulse system via a polarization selective beam splitter (19) and may be further used for frequency stabilization (see chapter 3.1.2). The cw light was frequency doubled by the nonlinear cristal (7) and further guided to the wavelength meter (3), which was calibrated by the laser light of the He-Ne laser (1). After the pulse shaping by the Faraday rotator (11) and the beam splitter (19) the laser pulses were amplified by four flash lamps instances with two amplifiers each (4). Afterwards they were frequency doubled by the nonlinear crystals (7) and further guided through the oven (14). Then the laser power was measured by a power meter (15). Since the largest part of the Rayleigh signal is suppressed by the iodine cell so that only the flanks are partially transmitted as well as the short exposure time, the Rayleigh scattering process produces only a weak intensity signal. To increase this signal, the laser beam diamater was reduced by a combination of a convex lens with focal length of 60 mm and a concave lens with focal length of -30 mm right before the entry into the oven. The camera system was used as described in chapter 4.1, with the interference filter (6) behind the iodine cell (5) in a

slightly diverging light path.

4.4.2 Results

Since the exposure time of the camera is set to take only one laser shot at a time, the intensity level of the measured Rayleigh signal is even with the reduction of the beam diameter at room temperature only at about 430 counts above the dark level of the camera of 230 counts as seen in figure 41. Although the dark level is stable at 230 ±10 counts and can be measured and subtracted by taking a background image with the laser switched off, it disturbs the measurements with low grayscale values. After the correction of the background of each individual image, 50 images were summed up and divided by the laser power of the beams to reduce statistical errors and variations of laser power (see figure 42).

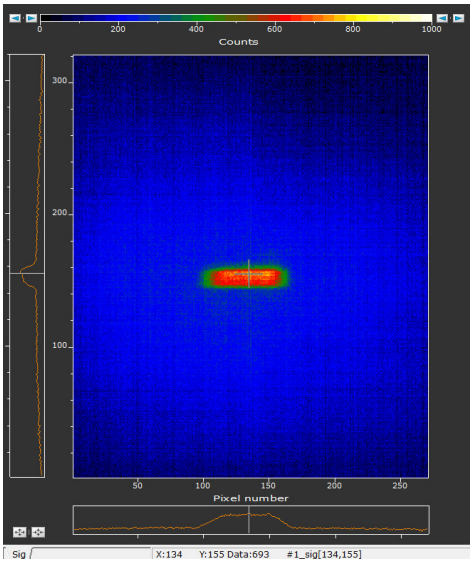

Figure 41: Image of a single laser shot without background correction.

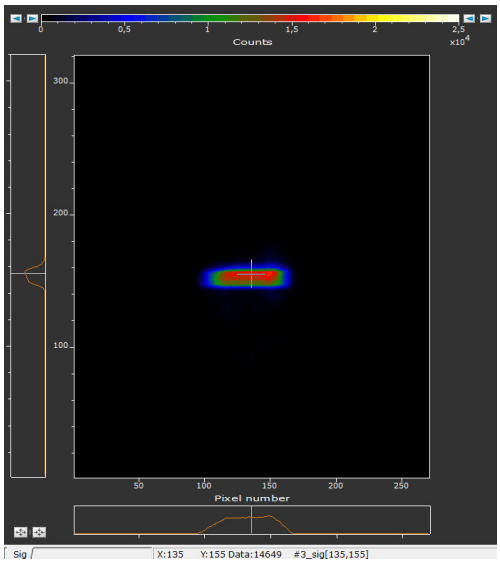

Figure 42: Image of 50 individual laser shots which were background corrected and afterwards summed up.

For the combined method (described in chapter 2.3.4) the laser is tuned from 18786.636 cm^{-1} to 18786.672 cm^{-1} with a step size of 0.002 cm^{-1} at the left stronger absorption line of the iodine spectrum to have 18 different intensity measurements. At the right weaker absorption line the measurements started at the wave number of 18786.750 cm^{-1} and is measured up to 18786.778 cm^{-1} with the same step size to have 14 separate measurements. However for the

evaluation only the images which show no contribution of Mie-scattered light were taken into account, to be able to neglect the B and B_0 terms in equation 6. Therefore the final interval to be used is from 18786.638 cm^{-1} to 18786.666 cm^{-1} on the left absorption line and 18786.752 cm^{-1} to 18786.778 cm^{-1} on the right absorption line. Before heating the oven, a reference measurement at known thermodynamic conditions was taken to prove the functionality of the system. Therefore the experiment is performed at room temperature, standard pressure and with zero flow velocity. The result is plotted in figure 43. Clearly to see is that the residuals on the left interval are all negative and on the right interval are all positive. Our conclusion is that the camera is not completely linear at these low intensities. The linearity tests of the S-CMOS camera in chapter 4.2 only covered the linearity of the camera above 2000 counts. However in this experiment the measured images show count levels of less than 1000 counts, therefore a linearity problem could be the case.

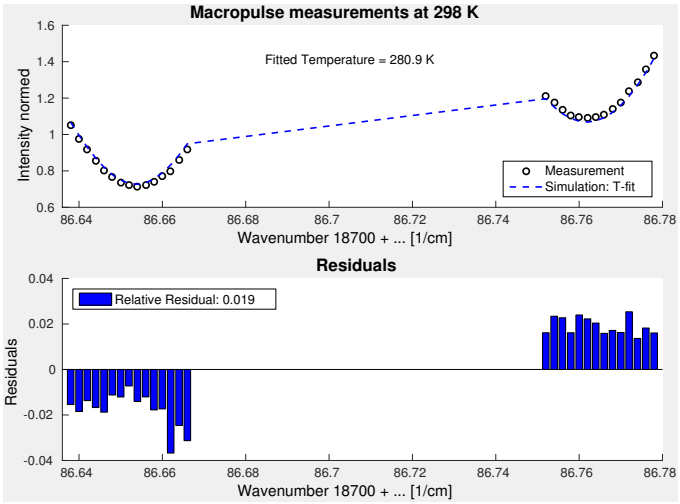

Figure 43: Measurement and evaluation of both absorption lines with the Macropuls system at room temperature. In the upper plot, the signal intensities for each laser frequency are plotted as black circles. The measurement was fitted using a Levenberg-Marquardt-algorithm (shown as a dashed blue line). The lower plot shows the deviation between the measurement and the fitting curve with the same normalization.

Since the left absorption line is slightly stronger than the right one, the intensity levels from the left are lower than the ones on the right causing a larger intensity range and therefore a larger error.
To minimize the resulting effect of this disadvantage, in figure 44 only the left absorption line is evaluated. Nevertheless an approximate temperature

difference of 15 degrees between the measured temperature between the thermocouple and FRS measurements remains. However this error was already found in previous FRS measurements and is handled as a constant offset to the actual temperature.

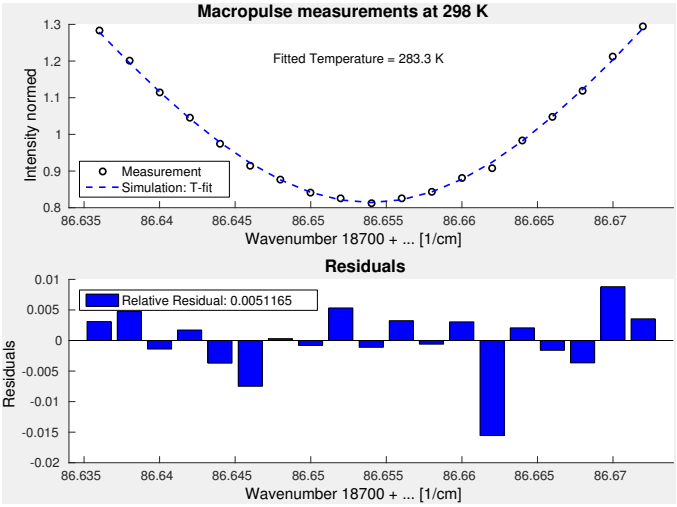

Figure 44: Measurement and evaluation of the left absorption line with the Macropuls system at room temperature. In the upper plot, the signal intensities normed to the reference measurement for each laser frequency are plotted as black circles. The measurement was fitted using a Levenberg-Marquardt-algorithm to determine the temperature (shown as a dashed blue line). The lower plot shows the deviation between the measurement and the fitting curve with the same normalization.

After the reference measurements, the oven was heated to 200, 400, 600, 800, 900, 1000 and 1100 °C. At each step both wave number intervals were measured five times consecutively and an average intensity value was calculated for each frequency. The resulting data sets were then fitted and the temperature was evaluated.
Hereby the combined method as mentioned in chapter 2.3.4 was used to determine the present temperature. This procedure worked well for temperatures up to 400 °C (for example see figure 45), but at 600 C (≈873 K) the evaluated temperature deviates from the one measured with the thermocouple by almost 24 % (see 46). We assume this is due to the use of the Tenti model for the description of the molecules' spectral response to incoming light.

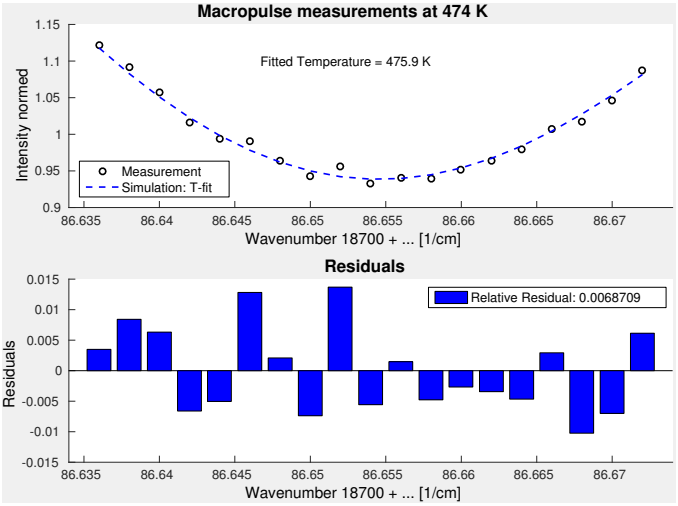

Figure 45: Measurement and evaluation of the left absorption line with the Macropuls system at 200 °C (≈473K).

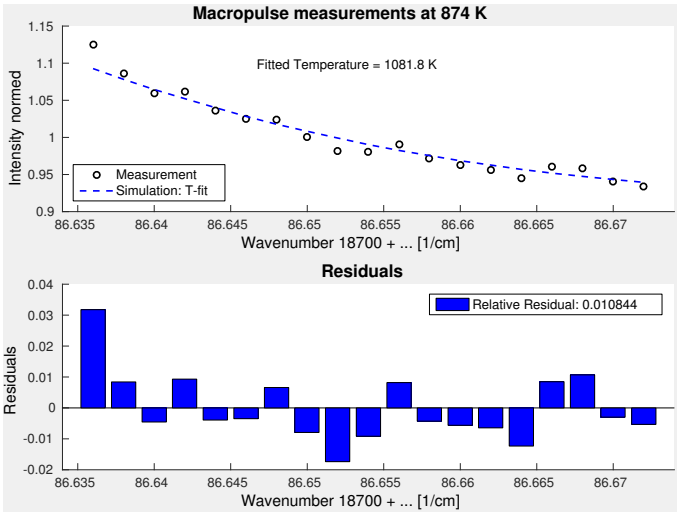

Figure 46: Measurement and evaluation of the left absorption line with the Macropuls system at 600 °C (≈873K).

This problem was already encountered in the dissertation [Dol16], in which an analytical model for the spectral response of the molecule ensemble at room temperatures was generated to reduce this error for FRS measurements. The Tenti model shows again better results for temperatures above 1000 °C. However at these temperature levels the signal intensity of the FRS signal dropped to less than 60 % of the intensity at room temperature. Due to

higher temperatures, the gas density decreased and thus the Rayleigh signal reduced. At these low intensity levels, the FRS signal is strongly impaired by statistical noise of the camera.

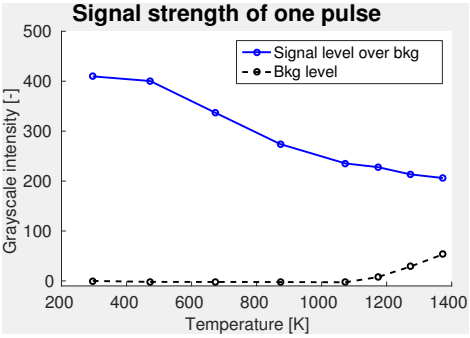

Figure 47: Development of the measured rayleigh signal with the temperature in a single Macropulse shot image (blue) and the development of the background signal due to black body radiation of the oven (black).

Figure 47 shows the decrease of signal strength for temperatures up to 1100 °C (1373 K) in blue. Also visible in this graphic is the thermal background level in black which only rises to a measurable amount at temperatures greater than 900 °C (1173 K) thanks to the short exposure time of 30 μs. Even at temperatures as high as 1100 °C (1373 K) the thermal background only contributes with approximately 70 counts and is therefore still far below the FRS signal intensity.

In a previous setup of this experiment, a different combination of lenses was used for the diameter reduction (parts 17 and 18 in the setup figure 40). These lenses were slightly too small for the laser beam to fit through and therefore created an interference pattern within the beam as seen in figure 48. Due to this diffraction pattern, the lenses were later changed to larger ones shown in the setup. However, in this setup the signal intensity of a single pulse image rose to approximately 600 counts above background contributions as in the other setup the intensity was only approximately 430 counts above background contributions. This last raise was enough to boost the quality of the measurement so much that even at the highest temperatures the oven could produce, namely 1175 °C (1448 K), the evaluated temperature was only off by about 1% (see figure 49).

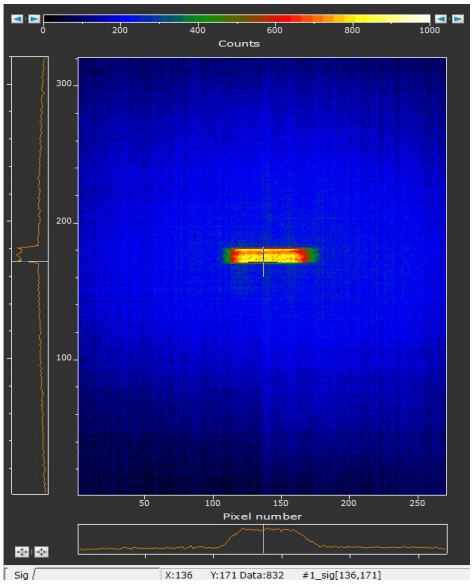

Figure 48: Camera image of the laser beam with the diffraction pattern.

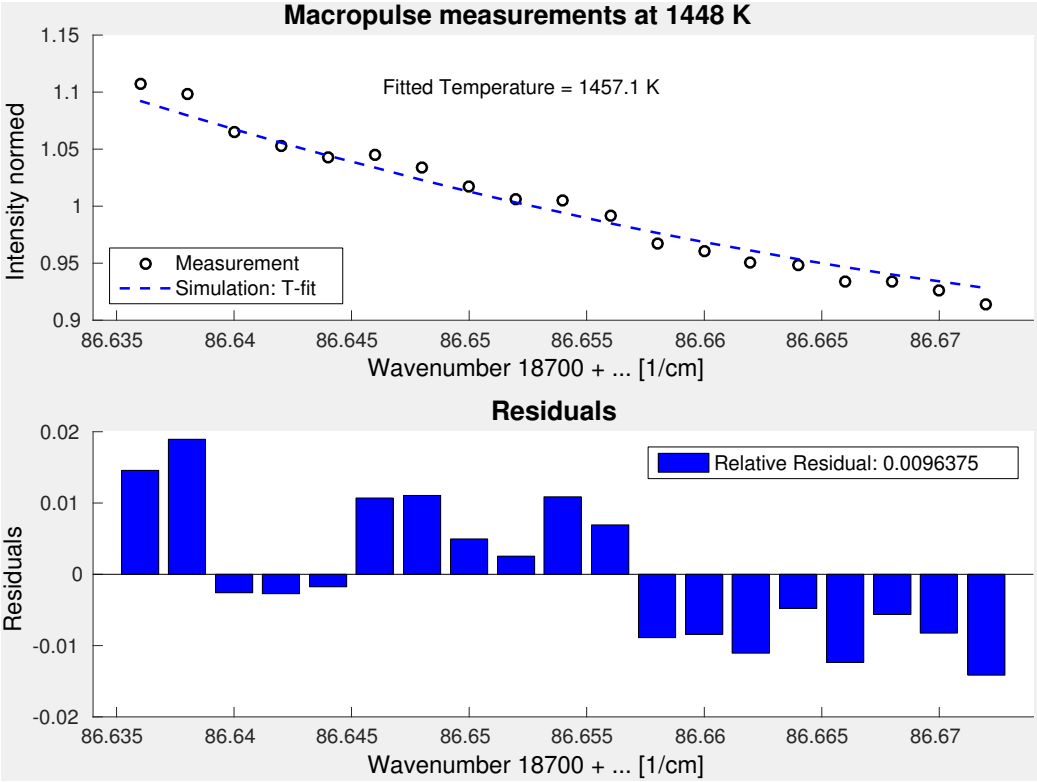

Figure 49: Masurement and evaluation of the left absorption line with the Macropuls system at 1175 °C (≈1448K).

4.4.3 Conclusion

The results from this experiment matched the temperature measured with the thermocouple only up to 400 °C with good precision and low residuals, due to errors in the spectral response shape of the molecule ensemble designed with the Tenti model. For temperatures higher than 1000 °C the model suits the real data fine again but the signal intensity dropped so far that statistical noise within the camera impaired an accurate evaluation of the signal. However the tests with the smaller lenses showed that with a higher intensity, even the signals at temperatures of 1175 °C showed good results. Therefore these measurements proved that the Macropulse system is now capable of taking conclusive data for temperatures up to 1175 °C with a low error of around 1%.

4.5 Analysis of *Alluxa's* 0.15 nm FWHM interference filter's spectral transmission profile

To improve the signal to background ratio of the measurements with the cw laser system at equivalent high temperatures as in the chapter before, two 0.15 nm FWHM bandpass filters were purchased (Their piece numbers were 3 and 6, therefore they will later be referred to as *Alluxa 3* and *Alluxa 6*). They should provide the system with a better spectral filtering than the 1 nm FWHM filter by *Barr* so that the influence of the black body radiation is suppressed stronger. The target is, that the FRS signal can be measured conclusively even with background temperatures of up to 1400 K. The central wave number[1] (CWN) of such filters can be shifted towards shorter wave numbers by raising the temperature of the filter. To test at which temperature the spectral transmission is highest following procedure was performed: First *Verdi's* frequency was tuned within its tuning range using the piezoelectric elements and for each frequency a transmission value was measured. After this series was measured, the filter was stabilized at a higher temperature and the same frequency region of the laser was measured. Due to the higher temperature, the filters transmission profile was shifted and another spectral part of the filter was observed.
The wave number region for FRS measurements contains two strong absorption lines in proximity to each other. The measurements were performed at the interval from 18788.324 cm^{-1} up to 18788.348 cm^{-1} at the left absorption line and 18788.42 cm^{-1} up to 18788.458 cm^{-1} at the right line. By using this method, the perfect temperature for the filters could be determined so that the transmission is highest in the region at which later FRS measurements were performed.

4.5.1 Setup

This setup seen in figure 50 was almost the same as the one used to check the linearity of the S-CMOS camera in chapter 4.2 except for the camera system (consisting of the components 5,6.1-3 and 15). In this experiment the camera system was composed of two camera lenses (6.1 and 6.2) with focal lengths of 75 mm for both. Next in line was *Alluxa's* interference filter (15), which was placed in an Aluminum ring and together set into an empty housing which is usually used to heat the iodine cells to the wanted temperature. Since the special housing mentioned in chapter 3.3 was constructed later, the filter was

[1] It is more common to speak of central wavelength (CWL), but since the precision for the experiments would have needed at least 6 decimal digits if expressed in wavelengths, wave numbers were the preferred unit.

stabilized to different temperatures with the use of this housing. After the filter, another camera lens (6.3) with a focal length of 100 mm was used to focus the incoming light at the S-CMOS camera (5).

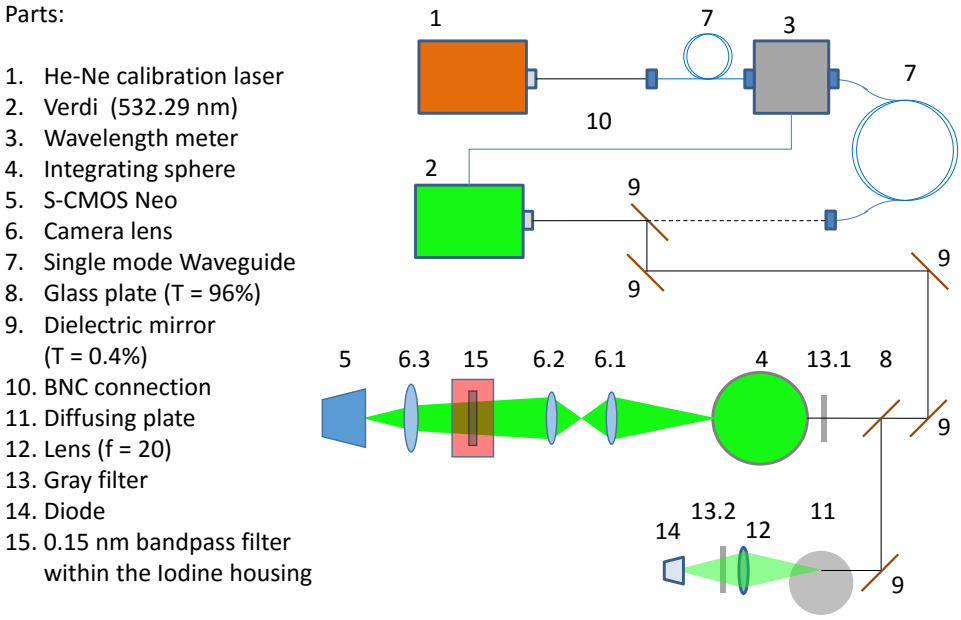

Figure 50: Setup of the transmission tests of the 0.15 nm FWHM interference filter.

4.5.2 Results

In this experiment a background image was taken first with the laser shut down. This image was then subtracted from all further measurements. Afterwards *Verdi's* power was set to 1 Watt and was three times for each temperature tuned from 18788.1 cm^{-1} to 18788.55 cm^{-1} with a step size of 0.5 cm^{-1}. At each wave number an image was taken with the camera. The camera's exposure time was 1 second and it was not binned so that the image sizes were 2160 x 2560 pixel. For the intensity values, a central area of 128 x 128 pixels was averaged. The range of the laser was kept constant, however the filter's temperature was raised from 23.5 °C, 30 °C, 40 °C, 50 °C, 60 °C, 70 °C and 80 °C, hence changing the effective transmission of the filter for the said wave number range. To visualize this effect, the data series were shifted to higher wave numbers, contrary to the direction, the filter's central wave number was shifted. The shifting factor was set so that the measurements would fit the theoretical transmission shape given by *Alluxa*. Figure 51 shows

the three measurement series for each temperatures. From this, an optimal temperature for the filter could be determined at which the transmission for the frequency interval between 18788.1 cm^{-1} to 18788.55 cm^{-1} was highest.

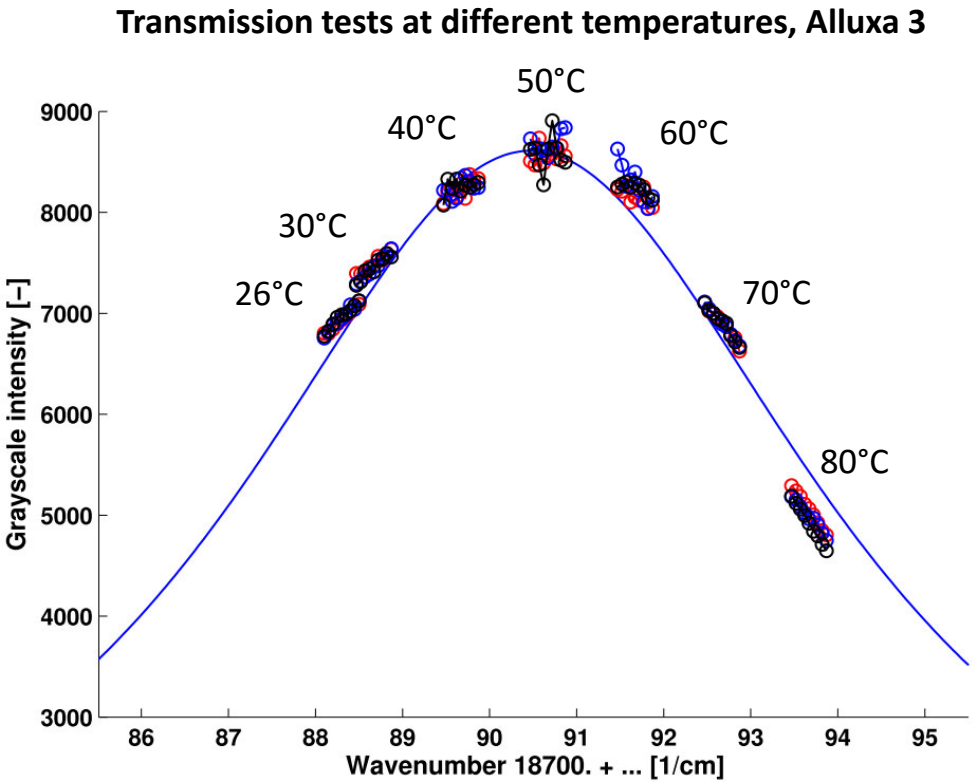

Figure 51: This figure gives an impression of the transmission shape of *Alluxa 3*. It was determined by 21 measurement series (7 temperatures times 3 measurement series for every temperature), in which the laser's wave number was tuned from 18788.1 cm^{-1} to 18788.55 cm^{-1}. The filter was heated to different temperatures, so that its CWN shifted and therefore the transmission changed. To visualize this, the series were shifted to higher wave numbers with higher temperatures of the filter. Therefore from left to right the temperatures of the filter at which the measurements took place are 26 °C (room temperature), 30 °C, 40 °C, 50 °C, 60 °C, 70 °C and 80 °C. The blue line is the theoretical transmission shape given by *Alluxa*.

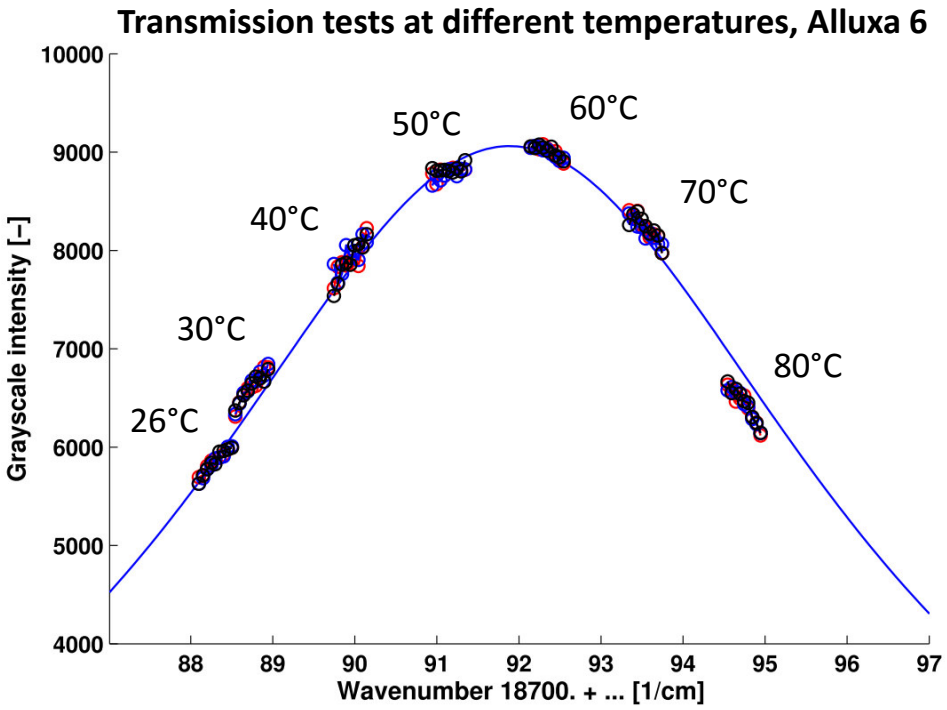

Figure 52: This figure gives an impression of the transmission shape of *Alluxa 6*. It was determined by 21 measurement series (7 temperatures times 3 measurement series for every temperature), in which the laser's wave number was tuned from 18788.1 cm^{-1} to 18788.55 cm^{-1}. The filter was heated to different temperatures, so that its CWN shifted and therefore the transmission changed. To visualize this, the series were shifted to higher wave numbers with higher temperatures of the filter. Therefore from left to right the temperatures of the filter at which the measurements took place are 26 °C (room temperature), 30 °C, 40 °C, 50 °C, 60 °C, 70 °C and 80 °C. The blue line is the theoretical transmission shape given by *Alluxa*.

4.5.3 Conclusion

It was concluded that the CWN of both filters were slightly too high for FRS experiments, since the transmission percentages of the filters were lower as expected at the wave number interval used for FRS measurements. But this experiment showed as well that the CWN of both filters could be shifted with reasonable temperatures to the desired wave number at which the FRS measurements could take place. The optimal temperature for *Alluxa 3* was 49 °C and for the *Alluxa 6* filter was 57.5 °C.

4.6 Determination of the angle dependent transmission profile of the molecular filter together with the interference filter

Since *Alluxa's* 0.15 nm bandpass filter has a Lorentzian spectral transmission profile (contrary to a flat top profile), even small angles will cause a change in the CWN of the filter, resulting in a decrease of the transmitted light's intensity. Since the camera has a non infinitely small CCD chip, the light path through the filter will have an increasing angle towards the edges of the image taken. To consider this contribution to FRS measurements, the transmission profile of the molecular absorption filter modified with the interference filter's transmission was measured.

4.6.1 Setup

Parts:

1. He-Ne calibration laser
2. Verdi (532.24 nm)
3. Wavelength meter
4. Integrating sphere
5. EM-CCD ImagEM
6. Iodine cell
7. Bandpass filter in thermal housing
8. Camera lenses
9. Single mode Waveguide
10. Endoscope
11. Glass plate (T = 96%)
12. Dielectric mirror (T = 0.4%)
13. BNC connection
14. Diffusing plate
15. Lens (f = 20)
16. Gray filter
17. Diode

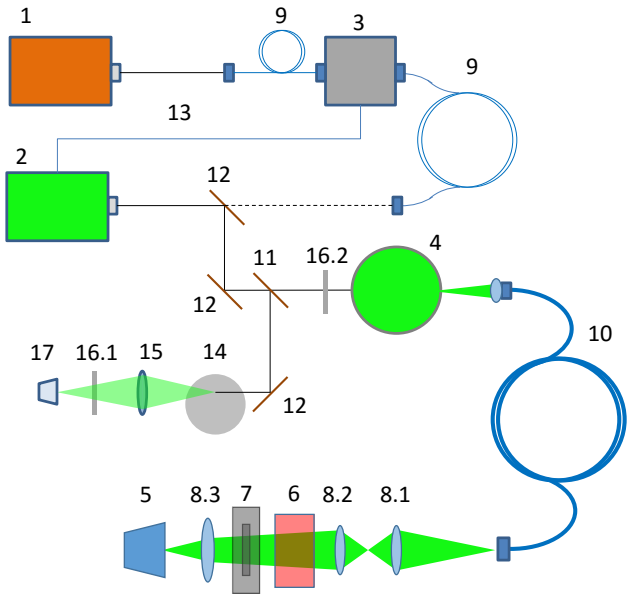

Figure 53: Setup for the determination of the angle dependent transmission profile of the molecular filter together with the interference filter.

For this experiment the setup in the previous chapter 4.5 was modified by using an endoscope (10) and putting the interference filter in the thermal housing (7) mentioned in 3.3. Also the camera was replaced with the EMCCD *ImagEM* and the molecular filter (iodine cell) (6) was placed in the camera system. The reason for the use of the endoscope was to test the system as it

would be used in measurements in gas power stations. In this environment an endoscope would also be used to have a view into the combustion chamber.

4.6.2 Results

For this experiment, the *Alluxa 6* filter was heated to 57.5 °C at which point the transmission of the wave number interval used for FRS measurements was best. The EMCCD camera was binned 4 times and an exposure time of 0.5 seconds was used. Before the experiment began, a background image without a laser source was taken to neutralize the dark level of the camera and background signals in later images. Then the laser was set to a power of 3 Watts to light the integrating sphere so that the camera was around 45000 counts peak (of a maximum of 65536 with 16 bit). Afterwards the laser's wave number was tuned from 18788.0 cm^{-1} to 18788.9 cm^{-1} three times with a step size of 0.002 cm^{-1}. These three series of 451 images were then averaged to have one mean image to every wave number, yielding a series of 451 images. This series of mean images were then saved in a 3 dimensional variable (height and width of the images times the number of all images 128x128x451). To determine the position dependent transmission profile from that, it is only necessary to pick a pixel position on the camera's chip (for example 64x64 for the center) and evaluate this three dimensional variable at this position (read out the one dimensional array left if the pixel is set to 64 in height and 64 in width for this example). That leaves an one dimensional array with intensity values. These need to be normalized by their maximal value and can then be assigned to the wave numbers of the original images. This process yields a final position dependent transmission curve of the molecular filter's transmission together with the interference filter's transmission.
Figure 54 displays an usual FRS signal image taken with this setup. Here the laser light produces Rayleigh scattered light. If this image is then evaluated at the 3 areas marked with the white rings, different transmission profiles need to be used to calculate back the original Rayleigh signal. These transmission curves are shown in the figures 56, 55 and 57.

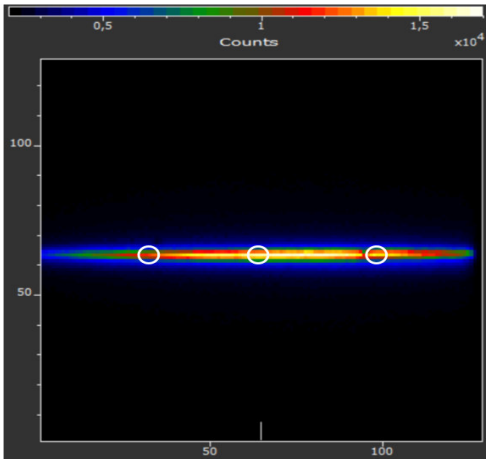

Figure 54: FRS signal image with Verdi through the endoscope. The image represents an usual FRS signal image in air which, if evaluated at different beam positions (white marked areas), need a different underlying transmission profile. These transmission profiles are calculated in this chapter.

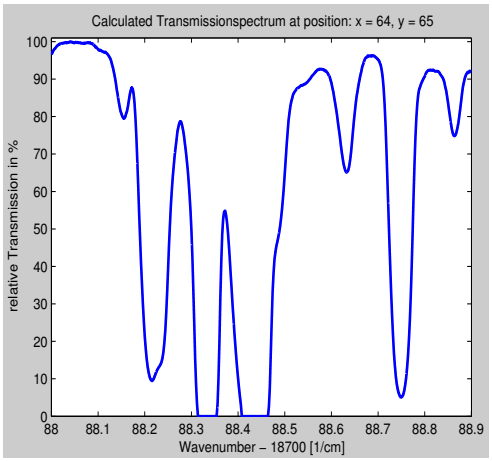

Figure 55: Spectral transmission of *Alluxa's* 0.15 nm interference filter at the center marked position of the laser beam.

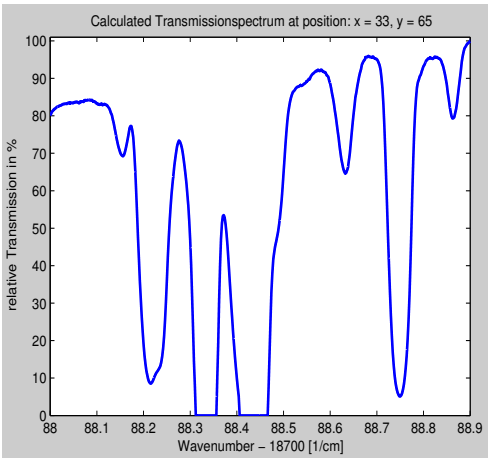

Figure 56: Spectral transmission of *Alluxa's* 0.15 nm interference filter at the left marked position of the laser beam.

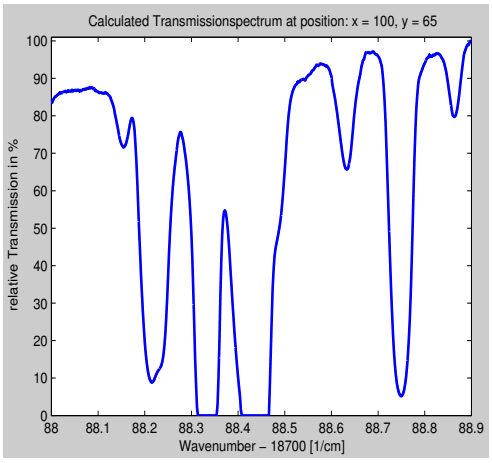

Figure 57: Spectral transmission of *Alluxa's* 0.15 nm interference filter at the right marked position of the laser beam.

4.6.3 Conclusion

In this experiment a camera pixel dependent transmission profile was created. As seen in figure 56 and 57, the transmission profile is indeed tilted, so that at the lowest measured wave number (18788.0) it is almost 20% lower as the transmission at the highest wave number (18788.9). However, in the center transmission plot (figure 55), the profile has nearly 10 % higher transmission at the lower limit than at the higher limit, indicating that the filter is heated slightly over its optimal balanced transmission profile in the center. This was a small trade off, since therefore the center transmission may have a slight drop to higher wave numbers, but the profile towards the edges of the signal picture have a less steep transmission profile as if the transmission profile would have been completely balanced from low to high wave numbers in the center.
This measurement is only valid as long as nothing in the camera setup (components 5-8) is changed, because of the high angle dependence of the filter. Therefore if FRS measurements are performed with any changes in the camera setup, these measurements need to be repeated for reliable results.

4.7 FRS measurements with the Verdi system in thermal background

For FRS measurements with the cw-laser *Verdi* the EMCCD camera *ImagEM* was used. Binning was set to 4 and the exposure time to 5 seconds to have an acceptable high signal level to evaluate. The laser's power in the experiment was 5 Watts and the interference filter was kept at 57.5 °C as in the experiment before. The experiment was carried out similar to the FRS measurements with the Macropulse system in chapter 4.4, so that at the beginning of the experiment a reference measurement was taken at room temperature. Afterwards the oven was heated and stabilized at the temperatures 200 °C, 400 °C, 600 °C, 800 °C, 850 °C, 900 °C and 950 °C. Then a set of three measurement series were taken in the wave number ranges of 18788.324 cm^{-1} to 18788.348 cm^{-1} and 18788.420 cm^{-1} to 18788.458 cm^{-1} with a step size of 0.002 cm^{-1}. Different to the measurements with the Macropulse system, here the background level was extracted from the signal images themselves. The intensity levels of two areas of 12 times 12 pixels were evaluated, one directly on the laser beam for the signal intensity of the Rayleigh light and the other one slightly above the laser beam for the background correction. Using this dynamic background correction, the dark noise level of the camera, the constant background of any other sources as well as a median level of the black body radiation throughout the exposure time was

subtracted from the signal level. After the measurements, the intensity levels to the corresponding wavelengths were fitted and the evaluated temperature was compared to the temperature measured with a thermocouple.

4.7.1 Setup

Parts:

1. He-Ne calibration laser
2. Verdi (532.29 nm)
3. Wavelength meter
4. Oven
5. EM-CCD ImagEM
6. Iodine cell
7. Bandpass filter in thermal housing
8. Camera lenses
9. Single mode Waveguide
10. Endoscope
11. Glass plate (T = 96%)
12. Dielectric mirror (T = 0.4%)
13. BNC connection
14. Diffusing plate
15. Lens (f = 20)
16. Gray filter
17. Diode
18. Beam dump
19. Thermocouple

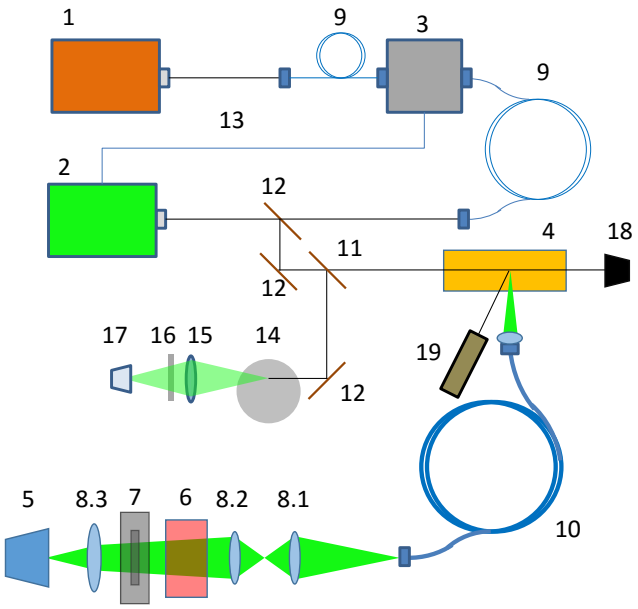

Figure 58: Setup of the FRS measurements with the cw-laser system *Verdi*.

As mentioned in section 4.6, to conduct FRS measurements with thermal background, the camera setup must not be changed, therefore only the integrating sphere was replaced with the oven (4) and the endoscope needed to be directed at the oven setup. After the laser passed the oven, the beam was dumped in a beam dump (18).

4.7.2 Results

For the FRS measurements with the cw-laser system also a reference measurement at room temperature, standard pressure and without flow velocity was performed to verify the systems performance. The measurement data was then fitted using the combined method. This evaluation returned a very

low mean residual of $\approx 0.3\%$ and a temperature which was only off from the measured temperature with the thermocouple by 6.1 K as seen in figure 59. Therefore the reference measurement was accounted for as a success and higher temperatures were tested.

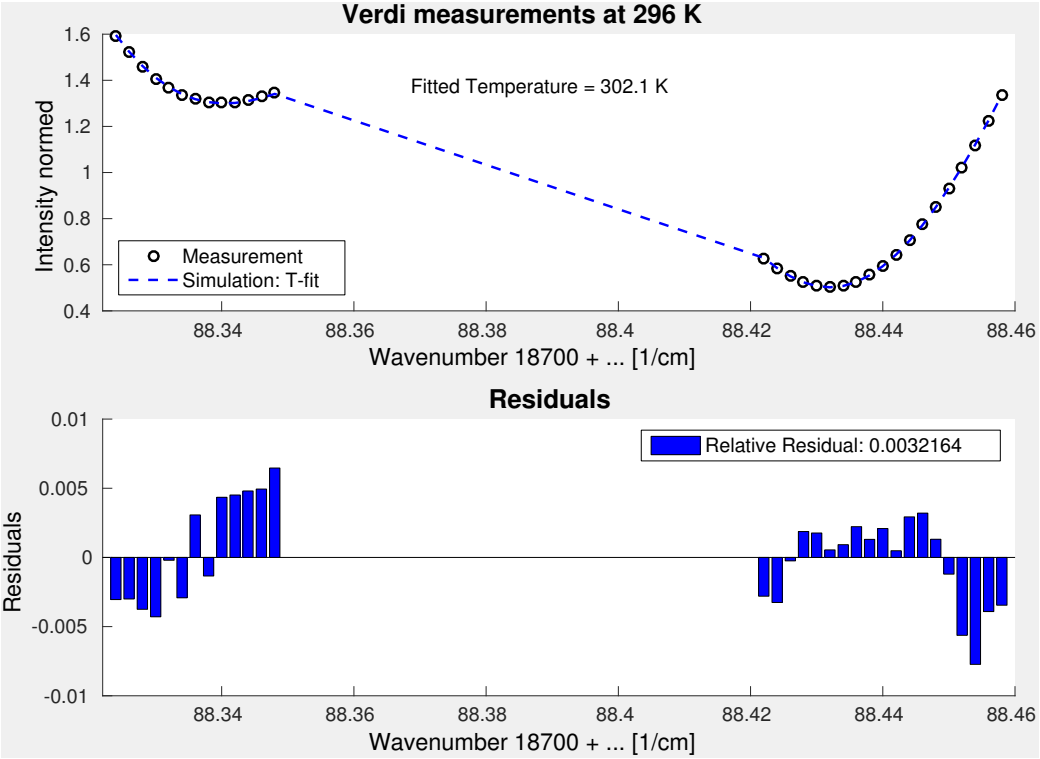

Figure 59: Reference measurement at known thermodynamic conditions to verify the functionality of the experiment setup. As before, the measurement data was normalized to its arithmetic median and is plotted in black circles. It was fitted using the Levenberg-Marquardt-algorithm plotted in a dashed blue line. The deviation of the fit from the measurement is shown in the lower plot.

For this purpose, the oven was heated with a large temperatures step size of 200 °C up to 800 °C and at each temperature three measurement series in the mentioned wave number regions were performed. The large temperature step size was chosen, since at these temperature levels the black body radiation was too low to be noticed. From 800 °C onward the step size was 50 °C up to 950 °C to see the growth of influence of the black body radiation as will be discussed later. The resulting measurement data normalized by the laser intensities is shown in figure 60. In this plot it is already visible that the intensity levels shrink significantly as the temperature was raised.

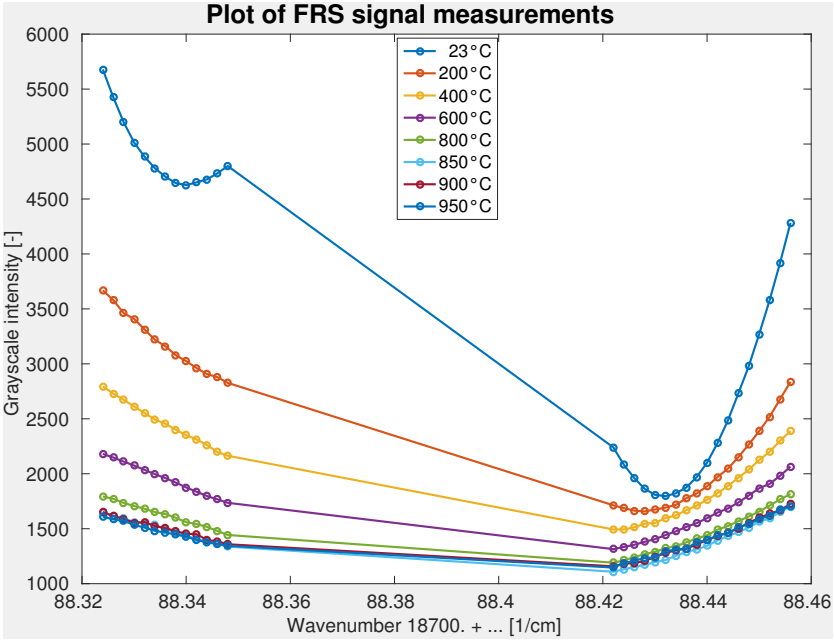

Figure 60: Plot of the different series of measurements at the given temperatures. Every measurement series seen here is the average of 3 individual measurement series normed to the laser power of each individual frequency at a set constant temperature. The wave number ranges chosen were from 18788.324 cm^{-1} to 18788.348 cm^{-1} and 18788.420 cm^{-1} to 18788.458 cm^{-1}.

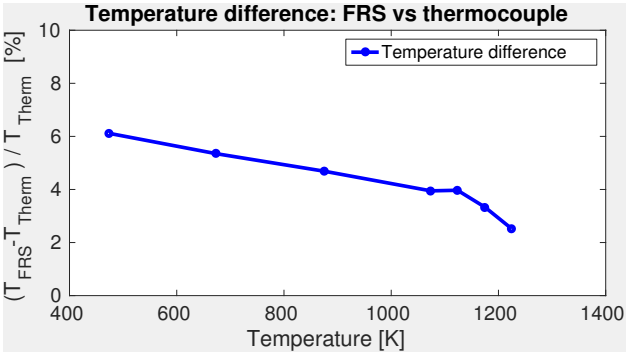

Figure 61: Development of the relative deviation between the fitted temperature and the measured temperature with the thermocouple in percent against the temperature.

Nevertheless throughout the experiment the temperature could be evaluated with decreasing deviations from 6.1 % at 200 °C down to 2.9 % at 950 °C. This was only possible because of the dynamic background evaluation as mentioned in the beginning of this experiment. Since slightest temperature variations at 950 °C resulted in a significant signal intensity fluctuation, the mean thermal background had to be subtracted from each single measurement point individually. Therefore the measurement data was

very smooth even at highest temperatures and could be fitted with a mean relative residual as low as $\approx 0.6\%$ from the theoretical curve as can be seen in figure 62.

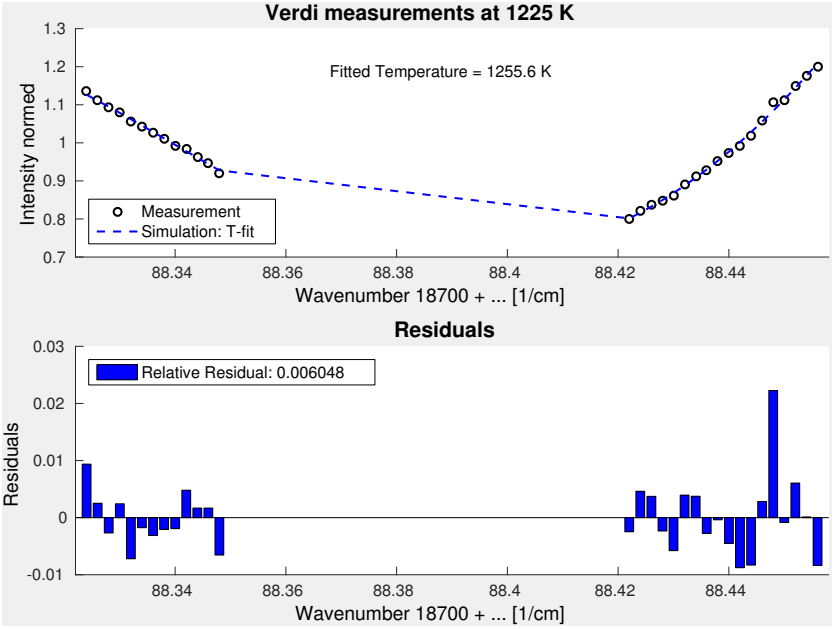

Figure 62: Measurement and evaluation of the signal data with the cw-system at 950 °C (≈1223K).

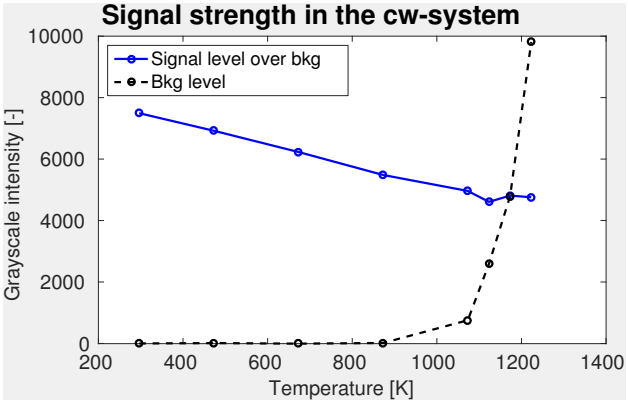

Figure 63: Development of the measured Rayleigh signal against the temperature in the cw-laser setup (blue) and the development of the background signal due to black body radiation of the oven (black).

Even though these measurements could be evaluated with high accuracy up to 950 °C, higher temperatures could not be measured as the black body radiation overexposed the camera chip due to its exponential growth (see figure 63). At the highest measured temperature 950 °C (1223 K) the thermal background was already twice as intense as the measurement signal.

4.7.3 Conclusion

Measurements with the cw-laser system were very successful with relative temperature deviations of only 2.9 % to 6.1 % to the absolute temperature. This system was able to measure the temperature up to 950 °C (≈ 1223 K) as it subtracted a dynamic background which lowered the influence of the black body radiation significantly as well as for the very narrow bandpass filter of only 0.15 nm FWHM. However higher temperatures could not be measured as the black body radiation overexposed the camera chip and therefore the signal intensity was not measurable.

5 Summary

In this thesis FRS measurements were performed with a pulsed laser system (chapter 4.4) and a cw laser system (chapter 4.7) to find out at which temperature the black body radiation of the oven would disturb the measurements enough to make the results impossible to evaluate.
Using the pulsed setup with the Macropulse system every single pulse of the laser was measured individually with a very low exposure time of the camera of 30 μs. Together with an 1 nm FWHM bandpass filter, the black body radiation was temporal as well as spectrally filtered. However since the Rayleigh signal is a very weak signal, the signal intensities measured in one pulse were very low and even sank with raising temperatures. Another systematic problem occurred around the region of 873 K. At this temperature level we assume that the Tenti model deviates from the real spectral response shape of the Rayleigh signal so that the measured temperature with the thermocouple showed a difference to the fitted temperature of 24 %. For temperatures above 1273 K the Tenti model fits the real spectral response better but at these temperatures the Rayleigh signal intensity sank so far that the camera noise level disturbed the measurements strongly. To improve the signal to noise ratio of the signal image, the camera program was modified to take 50 images of 50 consecutive laser pulses. After that they were normalized to the laser pulse power and summed up. Together with the improvement of the laser intensity by 40 % using an interference pattern, which emerged due to lenses smaller than the laser beam diameter, measurements at 1450 K could be evaluated with a relative deviation to the prevailing temperature of only 1 %.
For FRS experiments with the cw laser system a very long exposure time of 5 seconds compared to the 30 μs of the Macropulse system was chosen, to have a strong Rayleigh signal intensity. In this experiment the black body radiation was filtered with a very narrow bandpass filter with a FWHM of 0.15 nm. Since this filter's central transmission depends on its temperature and on the angle of incident of incoming light, two extra experiments were made. The first (chapter 4.5) was performed to determine the best temperature for the filter to have optimal transmission in the spectral region in which FRS measurements were performed and the second (chapter 4.6) to determine the spectral transmission shape of the molecular filter together with the interference filter in different regions of the signal image. After these tests, the FRS measurements with the cw laser system were executed and showed that using this system the temperatures could be determined with an average deviation from the temperature measured with the thermocouple of 4.5 % relative to the prevailing temperature.

Regarding the thermal background suppression in the systems, the Macropulse system was able to produce evaluable measurements at temperatures as high as the oven would go with 1448 K due to its temporal and spectral filtering. Even at this temperature level the background signal was still only at 70 counts in comparison to the Rayleigh signal level of 210 counts, yielding a signal to background ratio of 3:1 at 1450 K (see figure 47). Therefore the pulsed laser system suppressed disturbing black body radiation up to 1448 K good enough to allow FRS measurements at these temperature levels to be performed.
In the cw-system, the thermal background intensity reached the signal intensity level at 1175 K even though the very narrow 0.15 nm FWHM interference filter was used. Only 50 K more at 1225 K, the background signal was twice as high as the Rayleigh signal (see figure 63). The reason these measurements were still evaluable was that a dynamic background for every image was calculated, which subtracted the mean thermal background level throughout the exposure time of the camera from the signal image. At even higher temperatures the black body radiation overexposed the camera chip, so that the FRS measurement could not be evaluated. Therefore the cw-laser system as it was used in this thesis could measure the temperature up to 1225 K with a low mean deviation of 4.5 % relative to the prevailing temperature, but higher temperatures could not be measured.

6 Outlook

Since the measurements with the Macropulse system at temperature levels as high as 1450 K with very short exposure times of 30 μs for one pulse worked fine in the laboratory, this system is a very good candidate to be used in gas power stations to measure the temperatures of the molecules after the combustion of the gas and before the hot turbine vanes. In these measurements the laser beam will be guided into this area through a fiber and an image of the laser beam will be transmitted through an endoscope to the camera. The aim of this experiment is to detect the turbine inlet temperature, therefore the laser beam needs to be very close to the 1400 K hot vanes of the turbine. But since the Macropulse was able to measure the temperature even at a slightly higher thermal background, this setup shows great promise.
The cw laser system was able to measure the temperature conclusively up to 1225 K at exposure times of 5 seconds. To use this system it would be necessary to improve the spectral filtering even further as the 0.15 nm interference filter did. One solution to this problem would be to use a combination of a bandpass filter and a FabryProt etalon. This approach could be shrank down the spectral bandwidth of this combined filter system to a few GHz, improving the suppression of the blackbody radiation by a factor of 20. If this improvement is included into the experiment setup, also this system should be able to measure FRS signals with thermal background temperatures of up to 1400 K.

A Appendix

A.1 Master program

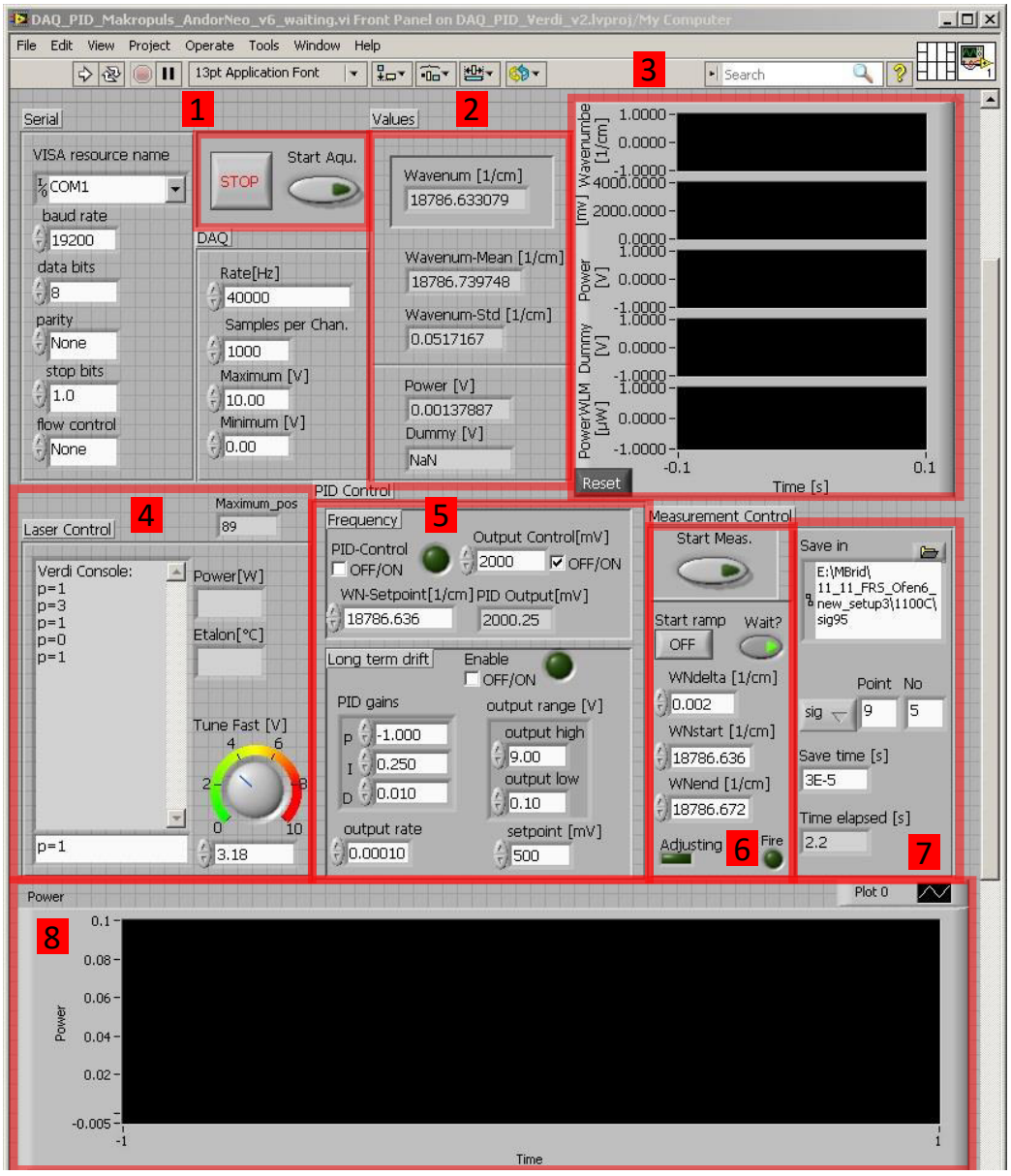

Figure 64: Graphical user interface of the LabVIEW program to adjust the laser's frequency, take signal images with the camera and save them into a folder.

The LabVIEW master program's grafical user interface is shown in figure 64. It is used for frequency scanning FRS measurements and its use and handling will now be explained for this purpose the red marked areas are inserted. After the program is started, the right button of the first area starts the acquisition. After this button is activated, the wavelength meter will measure the wave number of the laser and will feed the "Wavenum [1/cm]" display in area 2 with the currently measured wave number of the laser. Also the mean wave number and its standard deviation is calculated and filled into the displays in area 2. If a diode is connected, its generated power is shown in the "Power [V]" display. The power information can be lead back to the laser intensity and is also recorded in FRS measurements to normalize the signal intensity to the current laser power. In area 3 are wave charts from top to bottom of the courses of the wave number, the Voltage of the PID control of the wavelength meter, the power signal from the diode, an empty chart and the measured laser intensity at the wavelegth meter. Area 4 includes a console to issue commands to the *Verdi* laser using its RS-232 serial port, as well as a display of the set power and internal etalon temperature of the laser. The applied voltage to the "slow" access of the laser may be changed by the "Tune Fast [V]" controller in the right bottom corner of area 4. Area 5 contains the PID-controller of the wavelength meter. To activate the controller the top left check box needs to be checked. After that the wave number of the laser will be stabilized to the setpoint as determined in the "WN-Setpoint [1/cm]" box. To compensate for any temperature drift of the laser, the long term drift may be activated, which is able to modulate the voltage to the "slow" access. If the "Start ramp" button in area 6 is activated, the frequency scanning method will be applied. It will tune the lasers wave number to the one set in the "WNstart [1/cm]" box. After the laser is stabilized at the set wave number and the PID-output (in area 5) did not hit its maximum (4 V) or minimum (0 V) (implying that the PID controller was able to stabilize the laser to the setpoint) a measurement will start and the "Start Meas." button will be activated. If done so, the camera will expose its chip for the time determined in "Save time [s]" in area 7. As long as the camera chip is exposed the "Fire" indicator will be active. After the measurement, the image will be saved in the folder determined in area 7. If the PID-output did hit its edges, it could not stabilize the laser at the setpoint and an adjustment routine will start, activating the "Adjusting" indicator in area 6. It will raise the output rate (area 5) of the long term drift so that the laser may be adjusted using the "slow" access. During the adjust routine, no measurements take place. If the PID output (indicator in area 5 "PID Output [mV]") of the "fast" access is at its setpoint (controller in area 5 bottom right "setpoint [mV]"), indicating a successful stabilization of the

wave number of the laser at the "WN-Setpoint", the adjustment routine will deactivate and the FSM will continue. This program may also be used to work with the Macropulse system. Area 8 shows the course of a power meter for the pulsed laser system if one is connected. The plot uses a sampling rate of 40000 Hz to measure the voltage of the power meter. The 40000 signals are split up in 40 series of 1000 points. These 1000 points are plotted in area 8, therefore the plot changes with the same rate as the Macropulse laser shots (40 Hz).

A.2 Camera program

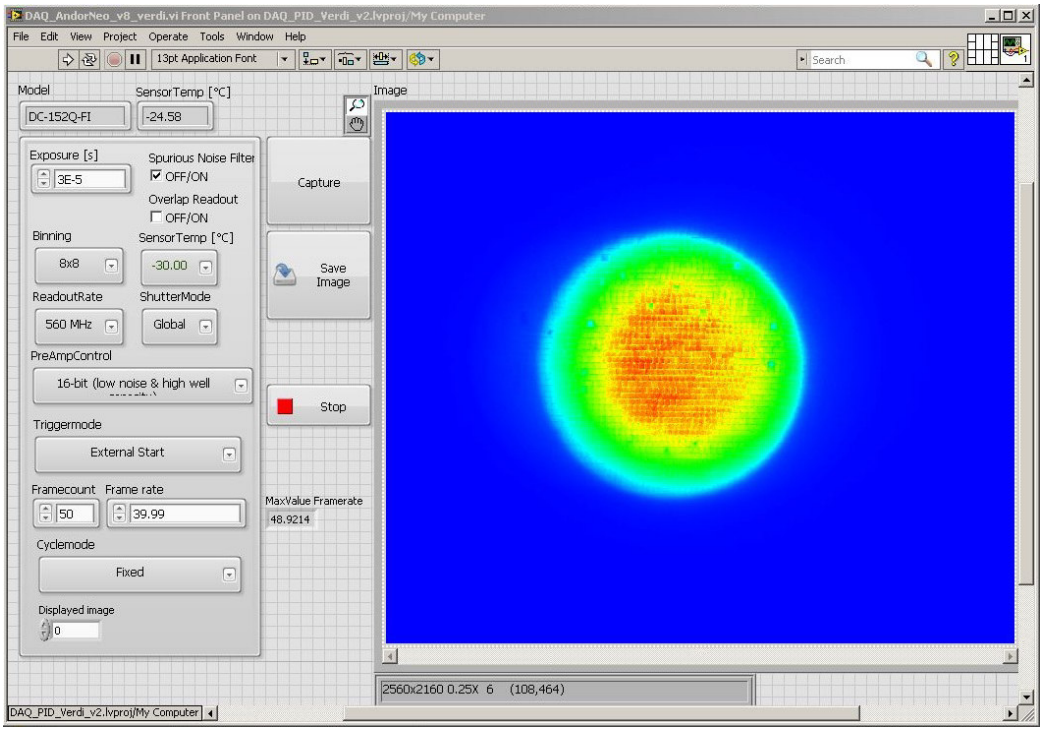

Figure 65: Screenshot of the GUI for the S-CMOS camera. On the left side is the console with handles to reprogram the camera and on the right side is a signal image in color coding.

The camera program seen in figure 65 controlled the S-CMOS *Neo* in the Macropulse experiments. This program needs to be configured before FRS measurements start and will during the frequency scanning method automatically be activated. This program allows the user to configure the following features of the camera: Exposure time (min: $9 \cdot 10^{-6}$s with global shutter

mode), binning (1,2,3,4,8), readout rate (200 or 560 MHz), the use of the spurious noise filter, whether to use an overlap of readout times, to which temperature the sensor shall be cooled (0°C, -10°C, -20°C, -30 °C), shutter mode (global or rolling shutter), which pre-amp gain shall be used (11- or 16-bit), the trigger mode (Internal, External, External Start, External Exposure, Software Trigger) and the cycle mode.
For experiments performed in this thesis 50 images of 50 consecutive laser beams were taken and therefore three additional features were included: Framecount, which sets the number of images taken in a kinetic record series, Framerate, which determines the rate, at which the images will be taken and a "Displayed image" handle to look through the raw individual images. This program also subtracts a constant background image from the raw images, divides by the measured laser intensity and sums up the 50 images. The resulting image can be shown if the "Displayed image" handle is set to 0.

References

[Bon12] Bonilla C., *The Effect of Film Cooling on Nozzle Guide Vane Ash Deposition*, Master thesis, 2012

[Vor02] Vortisch H.: *Observation of phase transitions in single levitated sulfuric acid solution droplets using Raman spectroscopy and elastic light scattering*, Dissertation, 2002

[Dol08] Doll U.: *Messung von Dichteschwankungen bei oszillierender Verbrennung mittels laserinduzierter Rayleigh-Streuung*, Diplomarbeit, 2008

[Mor05] Dr. Morherr, F.: *Strahlungsgesetze*, 2005

[Tenti74] Tenti G., Boley C.D., and Desai R.C., *On the kinetic model description of rayleigh-brillouin scattering from molecular gases*, Canadian Journal of Physics 52, 1974, Nr. 4, S. 285-290

[Dol16] Doll U.: *Gefilterte Rayleigh-Streuung zur simultanen Bestimmung von Druck-, Temperatur- und Geschwindigkeitsfeldern in Gasstrmungen*, submitted dissertation, 2016

[Yeh88] P. Yeh, *Optical Waves in Layered Media*, 1988

[Gu13] Ziyu G., Witschas B., van de Water W., Ubachs W.: *Rayleigh-Brillouin scattering proles of air at dierent temperatures and pressures*, 2013

[Wit11] Witschas B., *Analytical model for RayleighBrillouin line shapes in air*, 2011

[Mil01] R.B. Miles, W.R. Lempert, and J.N. Forkey, Laser rayleigh scattering, Measurement Science and Technology 12, 2001

[Thor] Thorlabs official website
http://www.thorlabs.de/newgrouppage9.cfm?objectgroup_id=1001

[For96] Forkey, J., Finkelstein, N., Lempert, W. and Miles, R.,*Demonstration and characterization of filtered Rayleigh scattering for planar velocity measurements*, 1996

[Fork96] Forkey. J., *Development and Demonstration of Filtered Rayleigh Scattering: a Laser Based Flow Diagnostic for Planar Measurement of Velocity, Temperature and Pressure.*, PhD thesis, Princeton University, 1996.

[For97] *Corrected and calibrated I2 absorption model at frequency-doubled Nd:YAG laser wavelengths.*, 1997

[Vet92] Vetterling W. T., Flannery B. P., Press W. H. and Teukolski S. A.: *Numerical Recipes in Fortran-The art of scientific computing*, Cambridge University Press, 1992

[Man1] *Wavelength Control and Locking with Sub-MHz Precision*, a description of the working principle of *Verdi* lasers by *Coherent*

[Man2] High finesse website, http://www.highfinesse.com/en/wavelengthmeter

[Gun03] H. Gunzler and H.U. Gremlich, *Ir-spektroskopie*, Wiley-VCH, 2003.

[Top] Description of the working principle of a HighFinesse wavelength meter. http://www.toptica.com/products/wavelength_meters.html

[Sut13] Sutton J., Patton R., *Seed laser power effects on the spectral purity of Q-switched Nd:YAG lasers and the implications for ltered rayleigh scattering measurements*, 2013

[Ger79] Gerstenkorn, S., Luc, P, *Atlas du spectre d'absorption de la molecule d'iode*, 1978

Ich habe die Arbeit selbstaendig verfasst, keine anderen als die angegebenen Quellen und Hilfsmittel benutzt und bisher keiner anderen Pruefungsbehoerde vorgelegt.